Centre for Geo-Information

Thesis Report GIRS-2005-33

UNMIXING - BASED IMAGE FUSION FOR LAND COVER MAPPING OVER THE NETHERLANDS

(A case study Landsat TM and MERIS imagery)

Maria Luz Guillén Climent

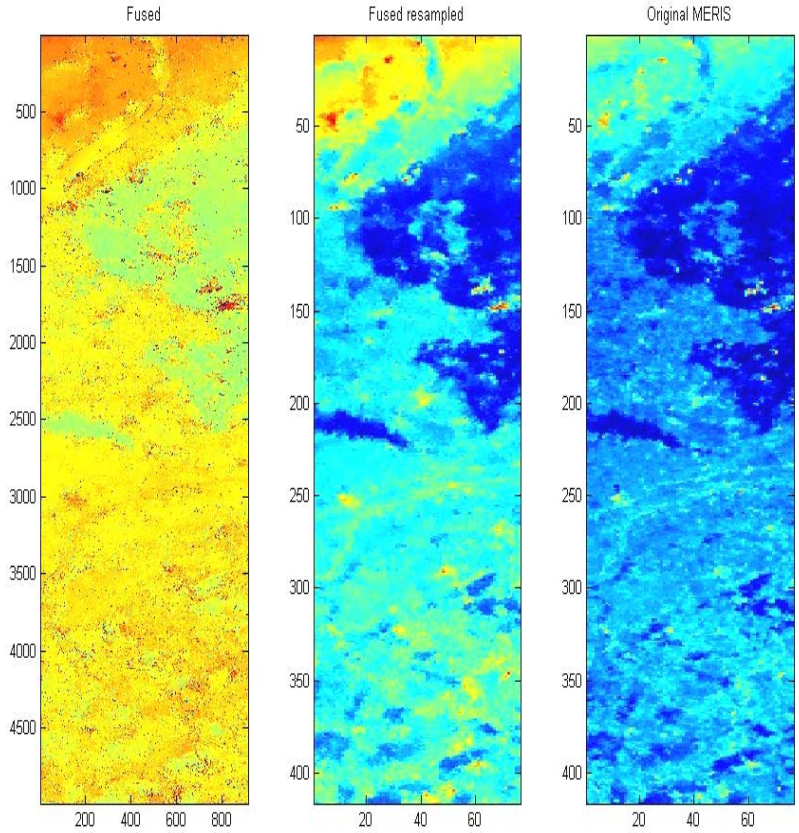

September 2005

WAGENINGEN UNIVERSITY
WAGENINGEN UR

Unmixing-based image fusion for land cover mapping over The Netherlands

(A case study Landsat TM and MERIS imagery)

Maria Luz Guillén Climent

Registration number 82 08 04 288 070

Supervisors:

Raúl Zurita Milla
Jan Clevers

September 2005
Wageningen, The Netherlands

Thesis code number: GRS-80430
Thesis Report: GIRS-2005-33
Wageningen University and Research Centre
Laboratory of Geo-Information Science and Remote Sensing

Acknowledgments

How time flies. I have been working on this research project for last seven months. During this time in Wageningen University I have met many people, both Dutch and foreign students. To work and live in this international group of students turned out to be the best learning experience of my staying in Wageningen. Thus, many people have participated in different ways on the development of this research. To all of them I would like to express my gratitude. First of all, I would like to thank Raul Zurita , for introducing me in the world of programming with Matlab and the data fusion, and also for his help not only in the work and Jan Clevers for their constructive criticism and supervision during this research.

I am also greatly indebted to Isabel Castillejo, because she was the first person in introducing me about something called Remote Sensing. And after a year of her first lesson, she has become a really good friend.

Of course, I cannot forget all my friends in Córdoba for their everlasting support. I know that they are there when I have needed something, and because of that they are so important for me. You are a lot of, and I can not put all your names, but special mention to Inma because she is an excellent friend in Córdoba and also my adventure friend in Wageningen.

Last but not least, this work is dedicated to my parents, my sister and Jose, who encouraged me throughout this period out of home. Thank you very much for your nice words in every moment and believe in me.

Thank you all

Abstract

A priority research in Europe is mapping and monitoring of land use and land cover (LUC). Actual and reliable information on LUC is needed both for agricultural and environmental applications. In The Netherlands was decided in 1987 to produce a national land cover/ use database ('LGN data base') using satellites images (Landsat TM and SPOT) and ancillary data. This database has been frequently used for different purposes in the fields of environmental protections, water management, nature conservation and physical planning on regional and national scales. The use of ancillary data supposes a time consuming and expensive task. Thus, the aim of this work was to study the possibility to reduce the necessity of extra information by using a fused image. The fusion was made by using images from high spatial resolution sensor, Landsat TM, 25m as pixel size and 6 bands and from high spectral resolution sensor, MERIS, 300m as pixel size and 15 bands.

Previously to obtain the fused image, the optimal spatial resolution between 25 and 300 m for detection the changes in land cover in The Netherlands was tested. A graph showing how the local variance of a digital image for a scene changes as the resolution-cell size varies and the use of landscape indices were the two approaches applied for the first objective of this study. Both studies showed the necessity of study the subpixel level in a MERIS image.

The performance of the fusion between images was made by a method proposed by Zhukov et al. (1999). The method is based on the classification of the high spatial resolution image succeeds in showing class boundaries clearly, afterward both images are overlapped and the different classes inside of a MERIS pixel can be unmixed. The unmix-algorithm is applied in the high spectral resolution image by using a sliding window. Parameters like the size of this window or the number of classes in which the high spatial resolution images should be classified were optimized. Statistical parameters and a quantitative index were used to check the quality of the fused image. Finally a supervised classification of the fused image resulted in a land cover map.

In summary, the proposed method performed well the fusion between Landsat TM and MERIS images. And a fused image obtained with parameters correctly optimized can be successful for a land cover classification.

Keywords: data fusion, remote sensing, MERIS, LGN, land cover mapping, subpixel level, optimal scale.

Acronyms

ALV	Average Local Variance
CA	Class Area
CN	Conditional Number
ESA	European Space Agency
IGBP	International Geosphere-Biosphere Program
IHS	Intensity, Hue, Saturation
Lsqlin	Constrained linear least squares
LGN	Landelijk Grondgebruiksbestand Nederland (National Land use Database in The Netherlands)
LSU	Linear Spectral Unmixing
MERIS	Medium Resolution Imaging Spectrometer
MSS	Multispectral Scanner
NP	Number of Patches
NLCSmoothreg	Non-linear constraint smooth regularization
PCA	Principal Components Analysis
PLAND	Percentage of Landscape
RS	Remote Sensing
SAG	Scientific Advisory Group
TM	Thematic Mapper

Table of contents

List of tables

List of figures

1. Introduction

1.1 Background

The last few centuries have been characterized by rapid rates of change in chemical composition of the atmosphere, ground water and soils. An increasing awareness of these issues and the fear of serious consequences for the welfare and survival of humanity have prompted the scientific community to establish major efforts to understand the causes and implications of these changes (Verstraete et al., 1999). Both national and international mechanisms have been established to protect the environment and to ensure sustainable use of natural resources, some of them are the International Geosphere-Biosphere Programme (IGBP) which began in 1986 or Kyoto protocol (1997) (Clevers et al., 2005;Verstraete et al., 1999). Information about land cover and land use is a very important component for environmental planning and it is in this context that remote sensing (RS) is able to contribute (Treitz and Rogan, 2004).

In this research the case of The Netherlands has been studied; the population density of this country has increased very much during the last decades, the environment is being clearly affected and therefore land cover and land use are being continuously modified. Information about these man induced changes is required to support environmental policy and physical planning purposes (Thunnissen and De Wit, 2000).
The sources of data for obtaining and updating this information have undergone changes and have improved during the last decades. Until the end of the 1980s, information on land cover/use was usually obtained from land-use statistics and topographical maps. These sources were having some problems such as land use statistics could not be obtained for areas with deviating boundaries, for example river basins, or topographical maps did not include all land cover/ use and they were not available in digital form. To overcome these problems, in 1987 it was decided to produce a land-cover database of The Netherlands in a raster format using satellite images. This is the so-called "LGN-database" (see chapter 3.1.3). Nowadays five versions of LGN are available. The last two versions, LGN4 and LGN5 are based on the following information:

- TOP10-vector, 1:10000 digital topographic vector map used as a geometric base reference.
- Landsat-TM imagery, and if these images are not available; IRS-LISS3 and ERS2-SAR provided the information (De Wit and Clevers, 2004)
- Ancillary data:
    - The PIPO system; is an administrative system that has been developed to check all acreage-based applications for subsidies.
    - Agricultural Statistics; the General Census of Agriculture which provides information of the acreage of crops grown.

Many sources of information are required and because of that the updating of the LGN is an expensive and time-consuming task. To facilitate this effort, it could be interesting to complement Landsat information with the information of other satellites providing more spectral information or high te,poral resolution.

The MERIS sensor was primarily designed for ocean applications but many researches have shown the possibility of this sensor for land applications (Clevers et al., 2004a; Clevers et al., 2002; Van Der Meer et al., 2000; Verstraete et al., 1999). However the use of MERIS directly for land cover mapping is not possible, because of its medium spatial resolution. The Netherlands is highly fragmented; it does not have large areas with the same land cover. If the target size is smaller than the ground sampling distance it is necessary to study at subpixel levels (Chang et al., 2004). For these studies, there are some research methods and techniques that have been proposed in the remote sensing literature. One of these methods is Linear Spectral Unmixing (LSU). It estimates the fractional contribution of the detected endmembers to each pixel in the image (Grana and D'Anjou, 2004), but sometimes the studies with this technique have turned out inaccurate. One of the causes of this inaccuracy has been that LSU considers the reflectance obtained from a surface including many land cover types to be a linear combination of the reflectance of these land cover types. But there are multiple reflections and transmissions between the leaf layer and soil, so it is not a linear combination of the reflectance (Borel and Gerstl, 1994; Ray and Murray, 1996).
Another possibility to extract subpixel information is Data Fusion. This method has the advantage, with regard to the previous one, which the geo-location of the different proportions of each land cover/ use within a pixel can be obtained. Image fusion refers to the synergetic combination of different sources of sensor information into one representational format; this single image contains a more accurate description of the scene than any individual source image (Bretschneider and Kao, 2000; Simone et al., 2002).

Different Data Fusion procedures have been developed during the last decades. Some of the most important data fusion procedures will be briefly described in the chapter 2.2.

1.2 Problem definition

Actual and reliable information on land use and land cover is needed both for agricultural and environmental applications. So, making a map with this type of information would be very useful for many planning and management activities concerned with the surface of the earth.
Nowadays, Landsat TM images and ancillary data are used for mapping and monitoring land cover/use in The Netherlands. An alternative (possibly better) source of information could be to make such a map with a combination of images from different sensors, so making a fused image. This multisource information can improve the interpretation and classification of satellites images (Amarsaikhan and Douglas, 2004). Landsat TM information is very useful, but it has some features that could be completed with another source of information. For example:

- The frequency of capturing data.

The frequency of capturing data of Landsat-TM is 16 days. The Netherlands is usually covered by clouds, which supposes the satellite image is not very useful these days. Because of this, one might not obtain images in a period of one or two months.

MERIS has the capability to measure each 2-3 days. This high revisit frequency could be very convenient to solve the cloud cover problem. MERIS high temporal resolution

is also very useful for monitoring vegetation development during a year, like for phenology studies. It can avoid spectral confusion, because different land use types can reflect similar radiation in a determined season but we may distinguish them easier at other moments.

- The spatial resolution.

The landscape of The Netherlands is fragmented, agricultural crops cover the half of the country (Van Oort et al., 2004) and it does not have large areas with the same land cover. Therefore, a satellite with a low resolution like NOAA-AVHRR (pixel size 1.1Km) is not very suited for mapping land cover types in the Netherlands. However, the NOAA-AVHRR images cover a large area and therefore the *mosaic* effect that is created when using Landsat-TM images can be avoided.
Medium resolution satellite data, like MERIS data, may be very important in filling the gap between the low resolution satellite data and the high resolution satellite data.

A main research objective, therefore, must be to find the appropriate scale at which the changes that we want to observe occur. Considerable improvements in the image interpretation accuracy could be achieved if there is prior knowledge about the optimal spatial resolution for remote sensing based inventory (Hyppänen, 1996).

- The spectral resolution.

Landsat TM has 6 spectral bands located in the visible, near and middle infrared, and although MERIS spectral resolution consists of 15 spectral bands, they do not measure in the middle infrared. They are located in the visible and near-infrared and in some case they provide similar information. Thus, bands 3 till 8, in the visible, are strongly correlated. Also bands 10 till 14, in the NIR, are correlated. Band 9 takes an intermediate position, making it a particularly interesting band of the MERIS sensor (Clevers et al., 2004b).The location of this band is in red edge region and it can provide very useful information about studying the chlorophyll content and other biophysical variables as a measure of plant condition.

Taking into account these considerations, it can be concluded that producing an image with the spatial features of Landsat-TM and the appropriated characteristic of MERIS would be very useful for getting an accurate land cover database. Minghelli-Roman et al. (2001) showed that Landsat TM images are useful for enhancing MERIS images.

1.3 Research objectives

The aim of this research is to develop a methodology to get land cover mapping over The Netherlands by integrating multi-sensor remote sensing data. More specifically, an unmixing based data fusion method (Zhukov et al., 1999) has been tested in this study.

1.4 Research questions

This main issue led us to investigate the following questions:

1. Which scale gives the best visualization of the study area?
2. Can one use landscape fragmentation indices to define the best scale to map land cover types in The Netherlands?
3. What are the advantages of using a fused Landsat-TM and MERIS image for over Landsat-TM image when mapping and monitoring land cover?
4. Which indicators can be used to assess the quality of the fused image?

1.5 Outline of the report

This document is articulated in 5 chapters. The first one deals with a general introduction and the presentation of the project which supports this study. Chapter 2 describes the fundamental topics that have been treated in this research. Chapter 3 deals about materials, the characteristic of two needed images to do the fusion between them, and the LGN which is a land cover of The Netherlands whose process of elaboration is trying to be optimized. In chapter 4 the most appropriate scale to fuse the image is calculated. In chapter 5 the process of data fusion is carried out and some conclusions and recommendations for possible improvements in the research are commented. Finally chapter 6 summaries conclusions of the research answering questions proposed in this chapter.

2. Literature review

2.1 Remote sensing and land cover mapping

Land cover and land use are continuously changing. Environmental researches have shown up the importance of updating and reliable information on land use and land cover (Clevers et al., 2004a; Mucher et al., 2000). The knowledge on these variables is required in many aspects of land use planning and policy development, as a prerequisite for monitoring and modelling land use and environmental change (Billah and Rahman, 2004). However, the comprehensive information on the types and rates of land-cover and land-use change, and the less evidence on the causes, distributions, rates and consequences of those changes, make that the ability to obtain this information a tricky task. Remote sensing is presented like a powerful tool capable of providing timely and cost effective information.

Remote sensing is the science of acquiring information about the Earth's surface by sensing and recording reflected or emitted energy and processing, analyzing, and applying that information. The process involves an interaction between incident radiation and the targets of interest. In the last three decades, the technologies and methods of remote sensing have evolved to include a suite of sensors operating at a wide range of imaging scales with potential interest and importance to planners and land managers. The initiation of significant research activities in remote sensing technology, data analysis and applications was in 1972 with the launch of Landsat-1. In 1984, with the launch of the Landsat Thematic Mapper (TM) it was produced a new remote sensing data source that provided higher spectral, spatial, and radiometric resolution data, which allowed research to be conducted with greater precision, over large areas (Rogan and Chen, 2004). Since then, many other satellites have been launched and new airborne sensors have become operational. Specifically, the sensor that has been studied in this research, MERIS, was launched in 2002. It is on board of ENVISAT, which is the largest Earth Observation spacecraft ever built (www2). It carries ten sophisticated optical and radar instruments to provide continuous observation and monitoring of the Earth's land, atmosphere, oceans and ice caps. And although MERIS primary mission was the measurement of sea colour in oceans and coastal areas, many studies are showing its use for land and atmospheric monitoring (see Chapter 3.1.2)

Following the availability of the new sensors, many projects began to employ image fusion techniques, fundamentally using panchromatic and multispectral information for improved land-cover and land-use monitoring (e.g. (Pellemans et al., 1993)). Data fusion was presented as a new process in order to obtain accurate detail of an area by using different sources of information. Different techniques of Data Fusion are expounded in the next section.

2.2 Data Fusion

Earth observation satellites provide data covering different portions of the electromagnetic spectrum at different spatial, temporal and spectral resolutions. Every remotely sensed image has a specific limit of its own spectral and spatial resolution and there is no ideal sensor that is highly sensitive to all wavelengths and yields spatially detailed data. Nevertheless an image taken with a sensor can be complemented for images from other sensors, thus a fused image is created (Park and Kang, 2004). Fused images may provide increased interpretation capabilities and more reliable results since data with different characteristic are combined (Pohl and Van Genderen, 1998). On the one hand, the high spatial resolution is necessary for an accurate description of the shapes, features and structures. On the other hand, depending on the application and the level of complexity of the observed scene, the different objects are better identified if high spectral resolution images are used. To integrate different data in order to get more information than can be derived from each of the single sensors alone is the aim of image fusion.
These images should be as close as possible to reality and should simulate what would be observed by a sensor with the same modalities but the highest spatial resolution. Lucien Wald, in his book *"Data Fusion. Definitions and architectures. Fusion of images of different spatial resolutions"*, defines three properties that the synthetic images must respect:

1. Any synthetic image once degraded to its original resolution, should be as identical as possible to the original image.
2. Any synthetic image should be as identical as possible to the image that the corresponding sensor would observe with the highest spatial resolution if existent.
3. The multispectral set of synthetic images should be as identical as possible to the multispectral set of images that the corresponding sensor would observe with the highest spatial resolution if existent (Wald, 2002).

In this research, Landsat TM and MERIS images are going to be fused. The fused image will have the spatial resolution of Landsat TM (25m) and the spectral information of MERIS, 15 spectral bands. To check the quality of the fused images, some indicators have been used (see chapter 4 for a better description).
Several methods of data fusion are available in RS literature. Table 1 presents a brief review of the most important ones.

Table 1: Data fusion methods

Data Fusion Method	Description	Implicate	Reference
IHS	Three multispectral bands R, G and B of low resolution image are transformed to IHS colour space. Replacing I with the panchromatic high resolution image information and performing an inverse transformation from IHS back to the original RGB space, the fusion image is obtained.	·These methods substitute panchromatic data by I or PC-1 directly; and not always produce the best final products if both images have little correlation. ·All spectral components except for the substituted one are left in the original low resolution. ·Distorting the spectral characteristic.	(Lillesand and Keifer, 2000) (Chavez et al., 1991) (Zhukov et al., 1999)
PCA	PC1 is replaced by the panchromatic image and retransformed back into original RGB space.		
Arithmetic combinations (BroveyTransform, SVR, RE)	$Fusion_i = \frac{Multi_i}{Multi_{sum}} \times Pan$ With i=1…n, and $Multi_{sum}$=*Multi 1* +…+ *Multi n*	·They were developed to visually increase contrast in the low and high ends of the histogram of an image. ·They should not be used if we want to preserve the original radiometry information.	(Zhang, 2002)
Wavelet decomposition (LaplacianPyramid, FourierDecomposition)	The discrete wavelet transform (DWT) allows the image decomposition in different kinds of coefficients keeping the image information. Combining properly the different image coefficients, and through the inverse discrete wavelets transform (IDWT), the final fused image is achieved.	·They transfer high resolution information from a high spatial resolution image to the entire low spatial resolution spectral band. ·These techniques use the high frequency information directly, and may cause spectral distortion. ·They use big amount of data, sometimes they are out of physical domain.	(Pajares and de la Cruz, 2004) (www4) (Park and Kang, 2004)
Methods using adaptative windows	They apply nonlinear relationships between the images.	·They normally use only one band of high spatial resolution image. ·Zhukov´s method with the general case that the highest spatial resolution image may be multispectral.	(Moran, 1990) (Hill 1999) (Park and Kang, 2004) (Price, 1999) (Tapiador and Casanova, 2002)

The next flowcharts show the basic concept of some of the methods commented previously:

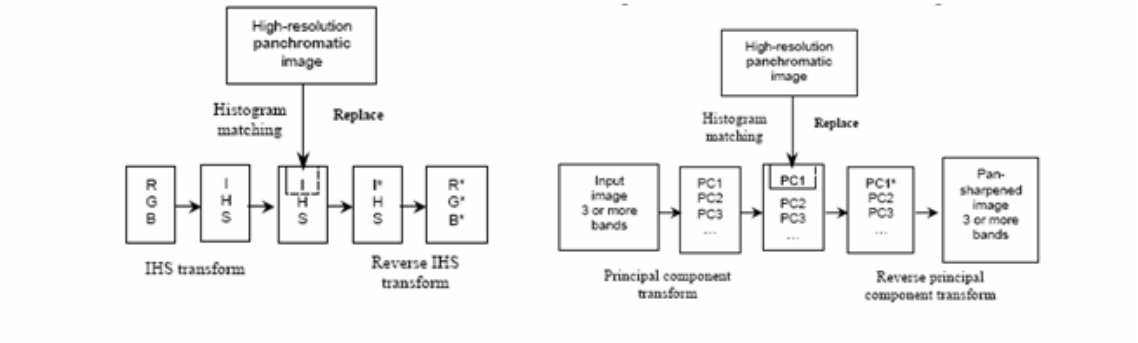

Figure 1:Schematic flowchart of IHS (left) and PCA (right) image fusion (Zhang, 2002)

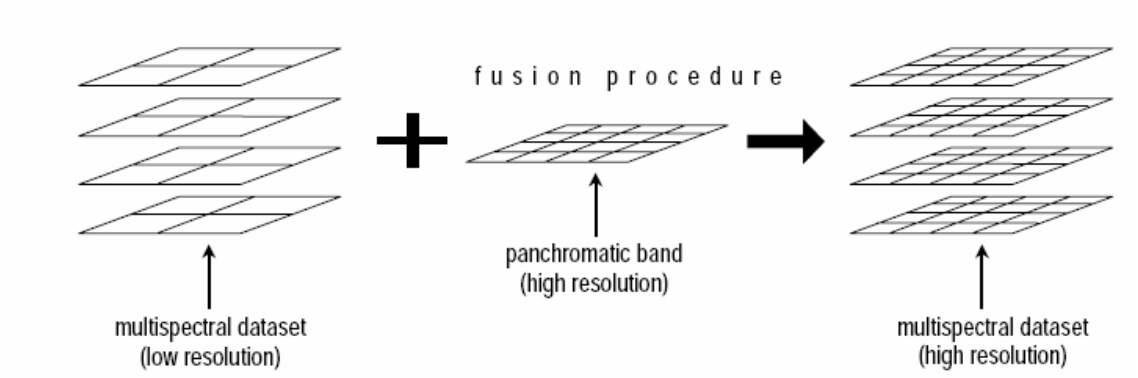

Figure 2: Concept of data fusion for resolution enhancement (Hill 1999)

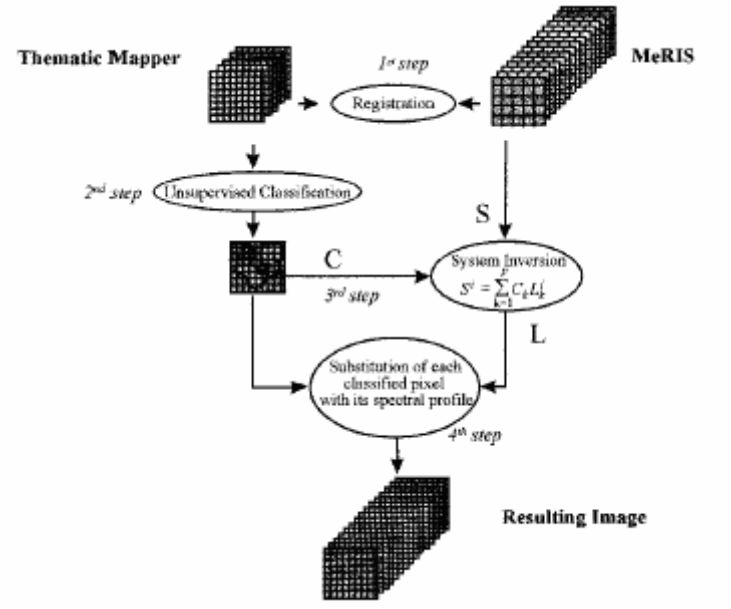

Figure 3: Fusion of two multispectral images (Minghelli-Roman et al., 2001)

Very well known techniques are IHS (intensity, hue, saturation), PCA (Principal components analysis), arithmetic combination based fusion and wavelet based fusion. However, a common problem associated with these techniques is the colour distortion of the fused image and that the fusion quality is operator and data dependent (Zhang, 2002, 2004). These techniques have been applied to the Pan image of the SPOT and IRS sensors, but they do not obtain an accurate quality in the image for new satellite images like Landsat-TM, IKONOS or Quickbird (Zhang, 1999). The techniques based on adaptive windows try to preserve the original spectral information. Especially Zhukov's methodology, the followed method in this research, presents the advantage with regards to the others that we can get information for all bands in the high spectral resolution image. It is not necessary to match bands belonging to the higher spatial resolution satellite with bands from higher spectral resolution satellite that cover a same spectral range.
This technique is proposed for unmixing the data of a lower resolution "measuring instrument" by its combined processing with the data of a higher-resolution "classifying instrument". It allows to classify the data and to map the classes with the resolution of the classifying instrument and to retrieve the mean signatures of the classes, corresponding to the measuring instrument (Zhukov et al., 1995).

2.3 Spectral unmixing

A satellite image consists of a two dimensional array of individual picture elements called pixels. Each pixel represents an area on the Earth's surface and has an intensity value, represented by a digital number. This value is normally an average of the whole ground area covered by the pixel. Resolution of an image is constrained by the pixel size and this pixel size is determined by the instantaneous field of view (IFOV) of the sensor's optical system. IFOV is a measure of the ground area viewed by a single detector element for a given moment in time. A large IFOV implies, therefore, that the ground area represented in each pixel is more likely to contain a mixture of materials of interest. The resultant spectra are a mixture and are referred to as "mixed pixels".
A mixed pixel in an image can be the consequence of any of the following situations on the ground (Fisher, 1997):

- Boundaries between two or more mapping units (e.g. field-woodland boundary)
- The intergrade between the central concepts of the mappable phenomena (ecotone)
- Linear sub-pixel objects (e.g. a narrow road)
- Small sub-pixel objects (e.g. house or tree)

These situations are shown in figure 4.

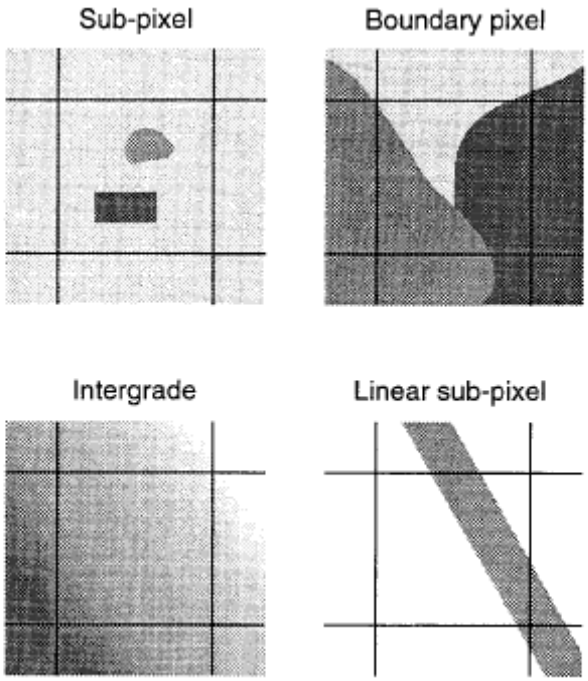

Figure 4: Four cases of mixed pixels (Fisher, 1997)

The presence of mixed pixels in applications such as performing a classification is a problem, since in conventional classification procedures the pixel is considered as an elementary unit for the analysis. Consequently, the subpixel level has to be studied. The mixed pixels require to be separated into individual constituents, called endmembers, whose radiances contribute to the single mixed-pixel value (Robinson et al., 2000). To transform the digital count of mixed-pixels into the digital count of the individual materials in that area of the scene is the purpose of the present study. The percentage of the individual material in the studied area is given by the higher spatial resolution image and the spectral signature of the classes present in a MERIS image will be obtained.

A method proposed by Zhukov et al. (1999) is used in this research to make the unmixing. This method applies the unmixing-algorithm in the high spectral resolution image by using a sliding window. The main steps followed in this method are:

- Georeferenced Landsat-TM images, with 25 x 25 m^2 as pixel size, are available from different dates. The first step is to make an unsupervised classification of these images. The unsupervised classification rule applied to these images was ISODATA.

Isodata unsupervised classification calculates class means evenly distributed in the data space and then iteratively clusters the remaining pixels using minimum distance techniques. Each iteration recalculates means and reclassifies pixels with respect to the new means. The number of iterations has been 50 and no distance threshold or standard deviation has been specified. Then all pixels are classified to the nearest class. This process continues until a number of 100 pixels in each class is reached (ENVI, 2004). The images were classified in 10, 20, 40, 60 and 80 classes. Afterwards, this number was optimized.

- The MERIS image was geometrically co-registered with the TM image. The pixel size of Landsat is 25 m and MERIS' pixel size 300m; therefore a MERIS pixel is matched to 12 by 12 Landsat-TM pixels (300/25=12).

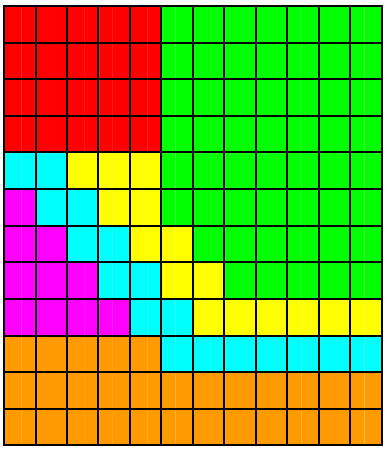

Figure 5: 12x12 Landsat pixels

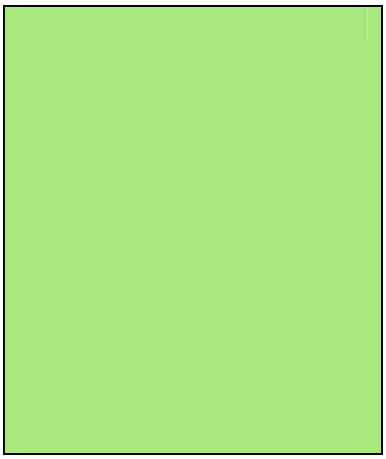

Figure 6: MERIS pixel

In general, there are more images from MERIS than from Landsat-TM; so more than one MERIS image will be co-registered with the same Landsat-TM image. Thus, multitemporal information of data fusion has been studied. The consequences of adding temporal information to the data fusion process have been evaluated in terms of overall classification accuracy.

- Using the classified Landsat-TM images as a reference, the proportion of each class at 25m will be calculated for each MERIS full resolution pixel (300m), in a window. The size of this sliding window will be optimized by testing different window sizes.

- Subsequently, the following algebraic system will be applied per pixel in the window to unmix the MERIS signal:

$$S^i = \sum_{K=1}^{N_c} C_K \cdot L_K^i + \varepsilon \quad \text{with} \quad i = 1,2,\ldots,nb_{MERIS}$$

Equation 1: System of linear mixture equations

C vector containing the proportion of each class within a MERIS pixel.

S^i radiance value of the ith MERIS spectral band.

N_c total number of classes.

L^i unknown vector containing the spectral radiance of each class in the ith MERIS spectral band.

n_{bMERIS} number of MERIS spectral bands.

Thus the unmixing is done for each band. In each band this equation is applied MERIS window by MERIS window to all pixels in the image. The restoration of the unmixed MERIS image is performed by assigning the estimated mean class signal to corresponding high-resolutions pixels of the classification maps, but the assignment is performed in each window only within the area of its central MERIS pixel. This is illustrated in the figure 7. We can distinguish 5 different classes in the window, in the first pixel appear two classes, to its right, the second pixel three classes, in the central pixel 4 classes. Once the equation is applied to each pixel, the signal of the five classes is obtained, but only the signal of the four classes corresponding to the central MERIS pixel will be assigned to the high-resolution pixels of the classifications maps in that area.

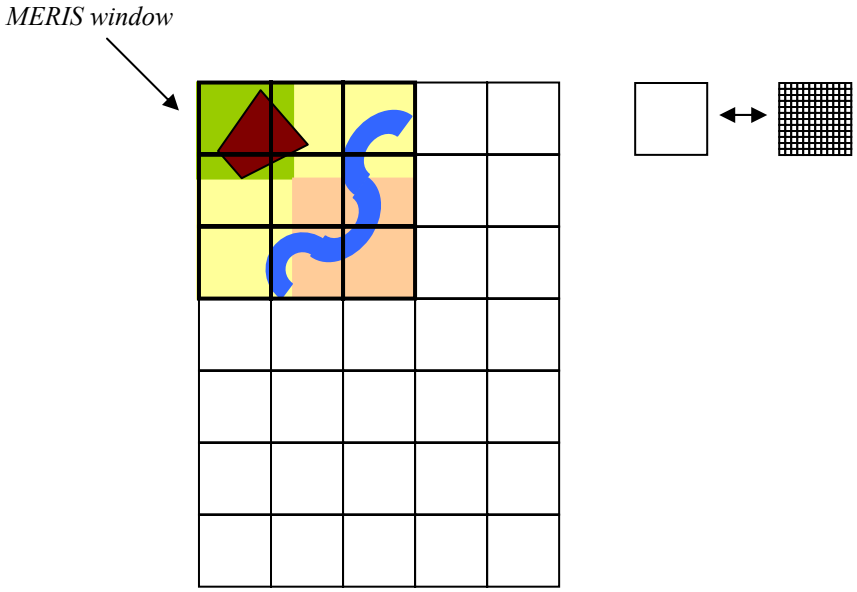

Figure 7: Applying equation 1

In the case that the number of classes in the window is higher than the number of pixels in the window there will not be enough equations for obtaining the unknown endmembers. Then, a bigger window should be used. The maximum number of classes in a MERIS window will be calculated, thus the window size can be optimized.

To avoid the effect of a frame when a window is used, the image will be padded with zeros. The size of this frame depends on the size of the window, being:
frame = (window size-1)/2.

The aim of this project is to get a fused image with Landsat TM and MERIS data, and to check if the land cover map obtained when that image is classified is more useful than a Landsat TM image.

3. Materials

3.1 Description of the available data sets

3.1.1 Landsat TM

For over 30 years, the Landsat platforms have been providing scientists with high-resolution satellite imagery. Landsat began the land mapping in the early 1970s with a series of 3 MSS (multispectral scanner) satellites that mapped using the three visible channels along with a near infrared band. In the early 1980s the next generation of Landsat satellites began offering what is known as the Thematic Mapper, which added two more infrared bands and a thermal long-wave infrared band, and doubles the resolution capabilities of the multispectral bands. The TM sensor is an advanced Earth resources sensor designed to achieve higher image resolution, sharper spectral separation, improved geometric fidelity, and greater radiometric accuracy and resolution than the MSS sensor. The TM data are scanned simultaneously in seven spectral bands. Band 6 scans thermal infrared radiation (www8). Spectral range of bands and spatial resolution for the TM sensor are given in table 2.

Table 2: Landsat TM resolutions

Bands	Range bands (nm)	Spatial resolution(m)
1	45-52	30
2	52-60	30
3	63-69	30
4	76-90	30
5	155-175	30
6	1040-1250	120
7	208-235	30

The primary objective of the Landsat project is to ensure a collection of consistently calibrated Earth imagery. Landsat's Global Survey Mission is to establish and execute a data acquisition strategy that ensures repetitive acquisition of observations over the Earth's land mass, coastal boundaries, and to ensure the data acquired are of utility in supporting the scientific objectives of monitoring changes in the Earth's land surface and associated environment (www9).

3.1.2 MERIS

MERIS (Medium Resolution Imaging Spectrometer) is a fine spectral and medium spatial resolution satellite sensor. MERIS is one of the core instrument payloads of Envisat, the European Space Agency's (ESA) environmental research satellite, launched in March 2002. MERIS operates in the solar reflective spectral range. It has 15 spectral programmable bands (capability of changing the band position and bandwidths throughout its lifetime) designed to acquire data at variable bandwidth between 1.25 and 30 nm over the spectral range 390nm to 1040 nm. Table 3 lists the current default bandset including variables that determined the final selection of band centre wavelengths and bandwidths.

Table 3: MERIS bands (Curran and Steele, 2005)

	Band		
Number	**Centre (nm)**	**Width (nm)**	**Environmental variables**
1	412.5	10	Yellow substance, turbidity
2	442.5	10	Chlorophyll absorption
3	490	10	Chlorophyll, other pigments
4	510	10	Turbidity, suspended sediment, red tides
5	560	10	Chlorophyll reference, suspended sediment
6	620	10	suspended sediment
7	665	10	Chlorophyll absorption
8	681.25	7.5	Chlorophyll fluorescence
9	708.75	10	Atmospheric correction
10	753.75	7.5	Oxygen absorption reference
11	760.625	3.75	Oxygen absorption R-branch
12	778.75	15	Aerosols, vegetation
13	865	20	Aerosols correction over ocean
14	885	10	Water vapour absorption reference
15	900	10	Water vapour absorption, vegetation

The instrument scans the Earth's surface by the so called "push broom" method. CCD arrays provide spatial sampling in the across track direction, while the satellite's motion provides scanning in the along-track direction. It is designed so that it can acquire data over the Earth whenever illumination conditions are suitable. The instrument has a 68.5º field of view around nadir, covering a swath width of 1150 Km with a spatial resolution of 300m at nadir. MERIS allows global coverage in 3 days.
The data are provided at 3 differents levels of processing- Level 0, Level 1 and Level 2 at two different resolutions- Full and reduced. The instrument always takes measurements with full resolution and onboard averaging generates the RR images (www2).

- Level 1, these products are images holding top of atmosphere radiances measured in the 15 MERIS bands.
- Level 2, they are provided with geophysical quantities varying according to the underlying surface identified (land, ocean or clouds).

Both products contain geometric information to locate the image on the Earth's surface; data describing the sun and viewing geometry; additional annotation data such as

coastline information; terrain height; meteorological data; scaling factors to decode the data from numerical geophysical meaningful values and flags that address the quality and the validity of the image.

MERIS was primarily designed for ocean and coastal zone remote sensing. However nowadays much broader environmental issues are addressed covering also land and atmospheric applications. The earlier objectives in 1987 of MERIS were:

Table 4: Earlier objectives of MERIS (Curran and Steele, 2005)

Ocean	Land
Scientifics and application oriented objectives 1. Chlorophyll concentration/ suspended sediment 2. Water quality/ dissolved organics 3. Shallow water depth/ bottom classification 4. Relationship between sea water optical properties and biophysical properties 5. Time series of biological and physical processes 6. Global radiation absorption by turbid water 7. Global and regional primary production 8. Pollution monitoring/ coastal processes	*Possible extensions to land applications* 1. Synoptical monitoring of vegetation indicators 2. Inland water bodies monitoring 3. Large scale (area) mapping

The MERIS Scientific Advisory Group (SAG) was composed principally of scientists with interest in ocean remote sensing and in the early 1990s more land and atmospheric scientists joined the group. Nevertheless, the ocean group was most involved in designing MERIS´s technical specifications and as a result these details were guided by ocean applications.

Land applications form only a modest contribution to the mission goal; nevertheless several researches have shown that MERIS has large potential for operational investigations over land areas (e.g.(Clevers et al., 2004a; Clevers et al., 2004b; Van Der Meer et al., 2000)). Its fine spectral and moderate spatial resolution could increase the capability to monitor terrestrial environments at regional to global scales, and fills the resolution gap between NOAA-like data and Landsat/SPOT-type data (Van Der Meer et al., 2000). These features joined to the repetitive acquisitions of such measurements should allow:

- Description of the dynamics of ecosystems.
- The quantification of deforestation and desertification processes.
- The monitoring of biomass burning and agricultural production.
- The documentation of land cover changes (Verstraete et al., 1999).

3.1.3 LGN

LGN is a spatial database that provides an overview of the crops that have been growing during a period in The Netherlands. It consists of raster cells of 25m by 25 m which cover the entire Netherlands, and for each cell land cover is determined. The first version was created in 1987 and since then four versions more have been produced, the most recent, LGN5, in July 2005. They are based on satellite images from 1986-2004. The database is widely used by national and regional government agencies for water management, hydrological modelling, land-use planning and environmental management (www1). For each update, the overall accuracy increased: LGN1 60% overall accuracy, LGN2 75% and LGN3 85% overall accuracy, 75% accuracy for individual classes. LGN1 and LGN2 were experimental databases with a limited accuracy and important shortcomings. In the third version those problems were quite solved and the use of LGN for ecological and environmental applications was strongly improved (De Wit and Clevers, 2004).
LGN4´s creation was realised by a methodology of classification that allowed to reduce costs, but to support high classification accuracy. A distinct advantage was the use of the 1:10000 digital topographic vector database of The Netherlands. The nomenclature of the LGN4 database contains 39 classes covering urban areas, water, forest, various agricultural crops and ecological classes and the accuracy requirement was similar to the LGN3 (85% overall accuracy, 75% accuracy for individual classes) (De Wit, 2003).
The production of LGN5 is comparable with LGN4. Legend and production process has been equal, offering the LGN5 database the possibility to monitor the changes for the period 1999-2004, since for this last update of the database satellite images of 2003 and 2004 have been used.
Both LGN4 and LGN5 aggregated into nine main land cover classes have been used in this study. These classes are: grassland, arable land, greenhouses, deciduous forest, coniferous forest, water, built-up areas, bare soil (including sand dunes), and natural vegetation.

For getting these nine classes, the LGN was resampled from 25 to 300m to match the MERIS FR pixel size. The aggregation method was based on using a majority filter with a kernel of 12 pixels (25m*12=300 m). The land use with highest abundance in the 12 by 12 kernel was used to label the new land use type (Zurita Milla et al., 2005).

3.2 Pre-processing data

A set of three Landsat TM and six MERIS images have been used in this research and for obtaining the final images the next steps have been followed.

3.2.1 Landsat images

The sensor Landsat, images from platforms five and seven have been used in the present study. The steps carried out have been:

- Change of format: They were acquired as ERDAS Imagine format comprised, they were decompressed and after converted to ENVI format. (To decompress the information the image was multiplied by 1.0 in ERDAS_MODELER).

- Geo-referencing: In addition to the change of format, the image was reprojected into the Dutch National reference coordinate system (RD). In The Netherlands all governmental offices concerned with spatial data use the national R.D. (Rijks Driehoek) coordinate system. It is stereographic map projection with its origin in Amersfoort (λ= 5º23'15.500'', longitude to the centre of projection, and φ=52º9'22.178'', latitude of the centre of projection) and the coordinates of the origin are shifted to X_0=155000.000 m and Y_0=463000.000 m.

- Study area: By using LGN as mask, a data set only covering the part of The Netherlands represented in Landsat images was extracted. Later taking into account the MERIS images, a smaller study area was selected.

Table 5: Landsat TM Acquisitions

Date (dd/mm/year)
28/03/2003
10/07/2003
11/08/2003

This research is divided in two main parts, and although both use Landsat images, there are some differences in the data set and also in the studied area:

(1) Justification subpixel level, where the optimal scale for the research is studied.
- Only Landsat image from 28 March 2003 is used.
- The size of the studied area is 1024 columns by 8096 rows pixels with 25 m of size.

(2) Process of the data fusion.
- Three Landsat images are used.
- The size of the studied area is smaller than the previous one, since MERIS images are used here, and there are some clouds in the North part. For this reason the size of the studied area in this part is 984 columns by 5064 or 4320 rows depending on the images.

3.2.2 MERIS images

For the research we were provided with a set of MERIS level 1 images. To fuse these images with the Landsat TM images, the dates should be as close as possible, thus the proximity between the dates and cloud free, were the main criterions to choose the MERIS image dates that we have used.
For the final MERIS images, the part of The Netherlands presented in the images was cut applying the same mask as used for Landsat TM images. Previously to this step, the image to be visualized in ENVI format with coordinates, GCPs were exported. In order to do this; the software BEAM 3.2 is used (new version 3.3 is already available).

The process followed:

1. In the software BEAM 3.2

   - To import ENVISAT products (MERIS images)
   - To obtain the geo-codes and export them as ENVI GCP.

2. In ENVI

   - The option Map ASCII Coordinate Conversion is chosen, where the next inputs have to be given: input projection (geographic lat/lon) and output projection (RD stelsel).
   - Finally, to warp the GCPs: Image to map, where polynomial 3rd degree and nearest neighbour were the selected options for obtaining the image with coordinates.

In this way the images could be overlapped and a common study area was chosen. The size of the final studied area is in Landsat image, 5076 rows by 984 samples, which is corresponding to 422 rows by 82 samples in the MERIS images.
Accordingly to Zhukov, it is very important that the images are perfectly co-registered, the co-registration errors should not exceed 0.1-0.2 of the low-resolution pixel size (Zhukov et al., 1999).

Another processing step was to transform the MERIS images from DN to radiances. For that the software EnviView has been used. EnviView is an application, which allows opening Envisat data file and examinees its contents. The information required is the value of the gains. The gains are used to optimise the sensor sensitivity, maximise the instrument resolution and prevent detectors saturation. There is a different value for each band.

$L=Gain*DN$

Equation 2: Transform DN into Radiance values

Where:

L: Radiance (mW/m^2/sr/nm)
DN: Radiometric value or digital number (0, 2^{16})
Gain=$\frac{L_{max} - L_{min}}{2^{16}}$;

Table 6: MERIS Acquisitions

Raw MERIS image	Sensing Start date	Procesed date
MER_FR__1PNIPA20030218_101833_000000982014_00008_05072_0094.N1	18/02/2003	02/04/2003
MER_FR__1PNUPA20030416_102705_000000982015_00323_05888_0177.N1	16/04/2003	19/07/2003
MER_FR__1PNUPA20030606_102410_000000982017_00051_06618_0176.N1	06/06/2003	19/07/2003
MER_FR__1PNEPA20030714_102918_000000982018_00094_07162_0139.N1	14/07/2003	05/08/2003
MER_FR__1PNUPA20030806_100639_000000982018_00423_07491_0465.N1	06/08/2003	25/08/2003
MER_FR__1PNEPA20030809_101258_000000982018_00466_07534_0279.N1	09/08/2003	29/08/2003

Another pre-processing that could be made to MERIS images by using the software BEAM is to correct the image for the smile effect. The BEAM Smile Correction Processor is aimed to enable the user to calculate smile corrected radiances from ENVISAT MERIS L1b products.
The images were corrected, but it was not possible with the MERIS image from 18th February 2003 due to the input is an old version and do not contain some data necessary for this process. For this reason, it was decided to work with MERIS images without smile correction. Nevertheless, in case that this pre-processing was done. In a sequential order the smile correction should be done at the beginning, before masking and exporting GCP´s.

Why the smile effect is produced?

MERIS is measuring the reflected sun light using CCD (Charge-Coupled Device) technique. A CCD is measuring in one of its dimensions one image line, and in the other dimension the spectrally dispersed radiance for each pixel along the image line. The spectral measurements of each pixel along an image line are made by its own set of sensors of the CCD. This causes small variations of the spectral wavelength of each pixel along the image. This is called smile "effect".
Five cameras each equipped with its own CCD sensor compose the MERIS instrument (see fig.8).The variation of the wavelength per pixel is in the order of 1 nm from one camera to another, while they are in order of 0.1nm within one camera. In processing algorithms which require very precise measurements the correction of this effect is necessary. Therefore, the MERIS Level 2 processor corrects the smile effect. The level 1b product is not smile corrected; this product provides the user exactly what the instrument is measuring (BEAM, 2005).

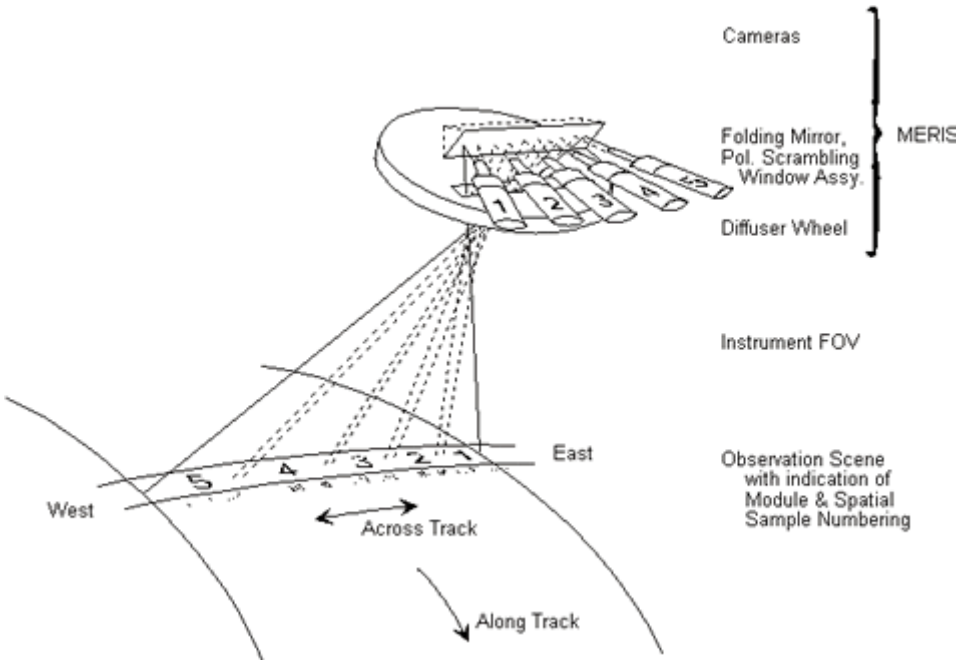

Figure 8: MERIS FOV, camera tracks, pixel enumeration and swath dimension(www2)

3.2.3 LGN

Five versions of LGN exist already. LGN4 aggregated into 9 classes (water, grassland, arable land, natural vegetation, deciduous forest, coniferous forest, greenhouses, built up and bare soil) has been the version used in the first part of the study because when this point of the analysis was being studied, in May 2005, LGN5 was not yet available. In the second part, for making the confusion matrices of the final classified images, LGN5 classified also in 9 classes was used as ground truth.

Finally, table 7 summarises the data used in each part of the research, data for optimal scale will be used in chapter 4, and for data fusion in chapter 5.

Table 7: Summary of images in the study

		Landsat TM	MERIS	LGN (9 classes)
Optimal scale		March 28th	-	LGN4
Data Fusion	**1st set fused dates**	March 28th	February 18th	LGN5
			April 16th	
	2nd set fused dates	July 10th	June 6th	
			July 14th	
	3rd set fused dates	August 11th	August 6th	
			August 9th	

4. Justification of subpixel level

This chapter describes all the steps carried out to test which is the appropriate scale for observing most of the changes in land cover and land use and the reason why we can not use the information of MERIS FR directly.

This study is composed of three phases addressing (1) Selection of study area (2) Application of a method using local variance and the use of landscape indices (3) Evaluation of the graphs obtained.

4.1 Methodology

4.1.1 Studied area

The Landsat image does not cover the whole of The Netherlands, so the images LGN and Landsat TM (28th March 2003) were cut with the same shape and then a studied area was chosen following the next criteria:

1. The studied area should be cloud free in the Landsat TM image.

2. The studied area should contain the nine land covers in which The Netherlands' landscape has been classified.

3. The size should be taken into account for the analysis.

The selected area covers approximately 25.6 Km by 202.4 Km, from 51º24' to 53º13' North latitude and 6º0' to 6º 22' East longitude. This is equivalent to 1024 rows by 8096 columns pixels with 25 m of size. This area represents The Netherlands' landscape; the nine representative classes appear in this zone and it is not covered by clouds.
The size of the image is important since the method using local variance to select an optimal scale computes the local variance of the images at different spatial resolutions, while still having a reasonable number of pixels to estimate local variance, there are a limited number of times that an image can be degraded (Woodcock and Strahler, 1987).
Figure 9 shows the selected area.

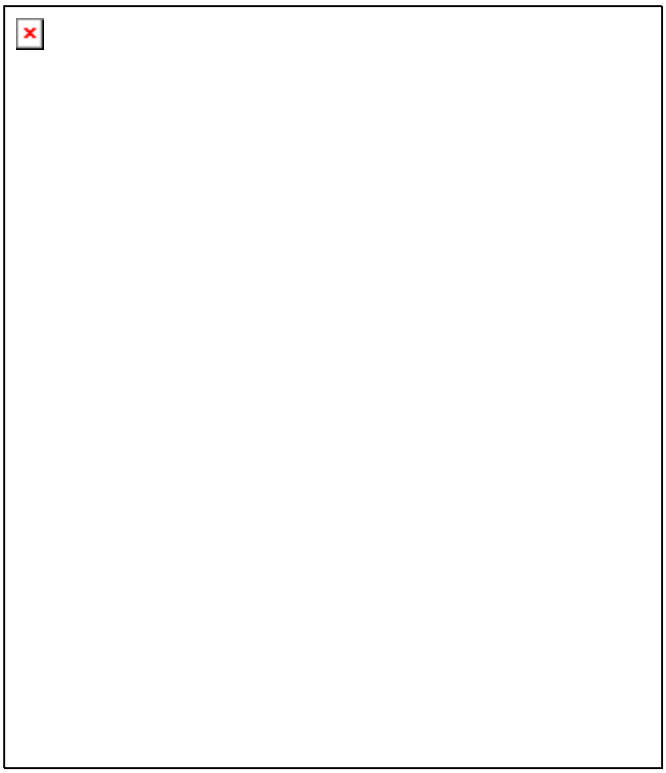

Figure 9: Studied area

Table 8: Percentage of each class in the studied area for Woodcock

Land cover	%
Grassland	43,76
Arable land	19,32
Greenhouses	0,06
Deciduous forest	6,01
Coniferous forest	10,84
Water	4,40
Built-up	11,78
Bare soil	0,39
Natural vegetation	3,43

4.1.2 Optimal scale applying local variance method

The methodology that has been followed is a technique developed by Woodcock and Strahler (1987). The local variance of the image is used as a criterion to know the appropriate spatial resolution which is needed for obtaining the information desired about the ground scene. Accordingly with the authors, if the spatial resolution is considerably finer than the objects in the scene, most of the measurements in the image will be highly correlated with their neighbours and a measure of local variance will be low. If the objects approximate the size of the resolution cells, then the likelihood of neighbours being similar decreases and the local variance rises.

A graph shows how the local variance of a digital image for a scene changes as function of the resolution cell size, and thus the spatial structure in the images is represented.
To measure local variance at multiple resolutions, the image data are degraded to coarser spatial resolutions. A consequence of this is that the number of pixels decreases as resolutions become coarser; for this reason, Woodcock, as a rule of thumb, proposes that the minimum size of images used to measure local variance should be around 60 pixels for have an adequate number of pixels to estimate local variance.

To apply this method, a MATLAB® application has been programmed. This application follows the next steps:

1. Choose the times that the scale of the original images is going to be degraded. Thus, if five steps are selected, the image will be degraded from 25 to 50, 100, 200, 400 and 800 m pixel size. For computing the pixel value after the degradation the mean between the pixels has been used.

2. The class to be examined is chosen. Each time that the program is executed, a graph for the relevant class previously selected is drawn.

The mean local variance of an image is computed using a sliding window of size N. N=3 is the window size recommended by the authors. The standard deviation of the nine values is computed, and the mean of these values over the entire image is taken as an indication of the local variability in the image. The function that executes the local variance is *mvarim_class*.
Firstly, the mean of the variance of the image without degradation is computed, afterward the original image is degraded and the successive local variances are obtained. Consequently the classified image, LGN, has to be degraded also; a function called *majority_filter* is used for this aim. This function makes a thematic aggregation of the classified image.
As it has been said before, each time that the program is executed only one class is examined, so for selecting it, we take solely the pixels bellowing to the chosen land cover.

The figure 10 shows the flowchart of this procedure. Two matrices are supposed to be the study area; the left one is LGN, each number corresponds with a land cover; to the right is the Landsat TM and the numbers are the DNs in each pixel. In this exemplification, the land cover named number 2 has been chosen, and only one step for the degradation has been represented.

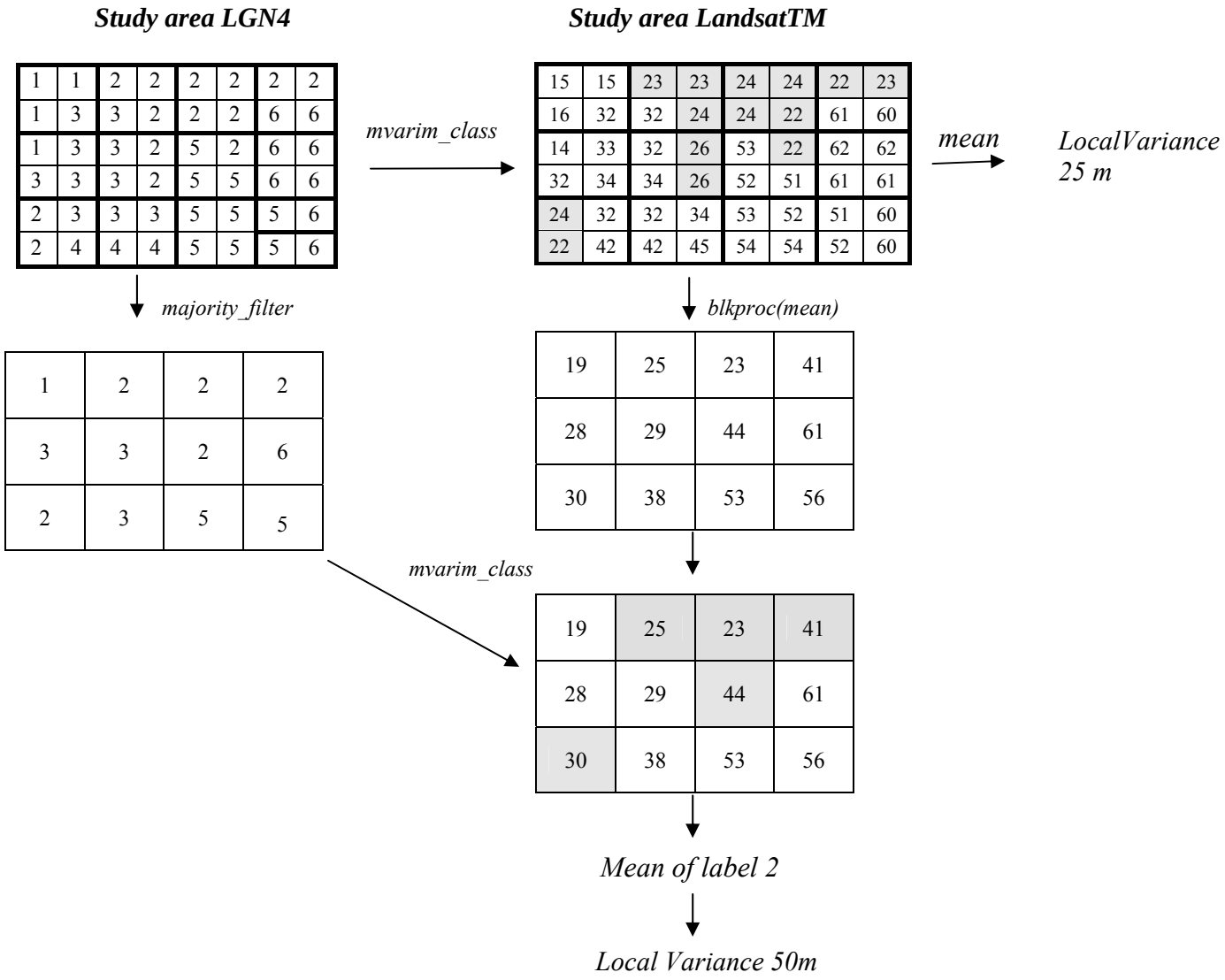

Figure 10: Flowchart Woodcock_MEAN

4.1.3 Optimal scale using landscape indices

The fragmentation of The Netherlands' landscape has been studied through landscape indices computed using "FRAGSTAT". FRAGSTAT is a spatial pattern analysis program for categorical maps; it quantifies the area extent and spatial configuration of patches within a landscape.

Our landscape consists of nine classes. For a given landscape mosaic, "Fragstats" computes several metrics at different levels: in each patch, in each class and in the landscape mosaic as a whole.
We have studied this landscape in terms of classes and patches. Indicative indices of the scale at which these classes can be observed, have been chosen.

Next the definition of these indices is given:

CA(ha); it is the total class area. It is equal to the sum of the areas of all patches of the corresponding patch type. This measure indicates how much of the landscape is comprised of a particular patch type.

PLAND(%); it is the percentage of landscape covered by a certain class. It is equal to the percentage of landscape comprised of the corresponding patch type. Percentage of landscape quantifies the proportional abundance of each type in the landscape.

NP; it is number of patches. It is the number of patches of the corresponding patch type.

LSI; it is Landscape shape index. Landscape shape index equals the total length of perimeter involving the corresponding class, divided by the minimum length of class perimeter possible for a maximally aggregated class. This index provides a measure of class aggregation.

$LSI \geq 1$, without limit
LSI=1 when the landscape consists of a single square or maximally compact patch of the corresponding type; LSI increases without limit as the patch type becomes more disaggregated.

The mentioned indexes have diferent relations with the level class. In the level of patches, the area of the patches has been computed. This index is very useful for the aim of this part of the research since we can see the number of patches with a determined area making up the studied landscape.

4.2 Results

4.2.1 Local variance

Nine classes comprising the landscape of The Netherlands were studied to check which the optimal scale for observing the different land covers is. The function programmed in MATLAB® was executed for each class. Graphs in figure 11 show the results obtained:

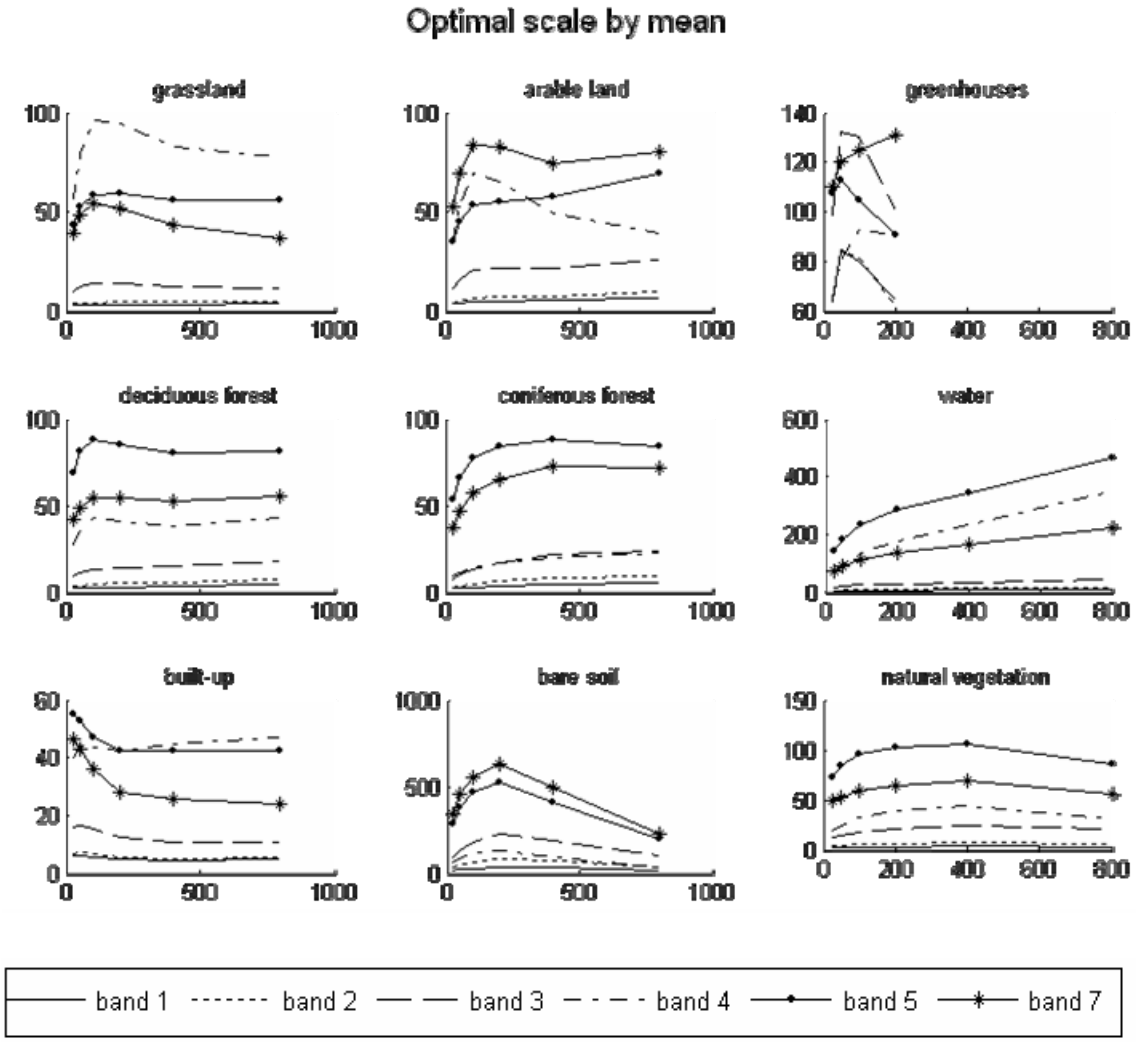

Figure 11: Optimal scale for different land covers
(X-axis: pixel size (m), Y-axis: local variance)

At first glance, the graphs do not show a clear result; nevertheless some conclusion can be obtained by examining graph by graph. Together to the information in table 9, these conclusions are commented.
Table 9 shows the pixel size where the local variance is maximum per band in the different classes.

Table 9: Pixel size where the local variance is maximum

	Band 1	Band 2	Band 3	Band 4	Band 5	Band 6
Grassland	800	800	100	100	200	100
Arable land	800	800	800	100	800	100
Greenhouses	50	50	50	100	50	200
Deciduous forest	800	800	800	800	100	800
Coniferous forest	800	800	800	800	400	400
Water	800	800	800	800	800	800
Built-up area	25	50	50	800	25	25
Bare soil	200	200	200	200	200	200
Natural vegetation	400	400	400	400	400	400

It was expected that the optimal resolution was land cover and wavelength dependent, but it has not been like this for many of the classes.

Three reasons could explain the incoherence between the different bands:

1) The spectral confusion between land covers in some bands.

Taking into account the reasoning of the authors about the relationship between local variance and spatial resolution. It can be concluded that in bands where the local variance is very low and the maximum is reached in pixel size of 400 or 800 meters, there is spectral confusion between different land covers.
For example in the case of arable land in the band 5, the maximum in the local variance is 800 m. This means that there is more than one class that has the same spectral behaviour in this band, since in a pixel of 800 by 800 it is highly probable that there exists more than one class mixed.

2) Low number of pixels to compute local variance

It was commented before that a minimum number of pixels to measure local variance should be 60. The size of the images decreases in the following way:

Table 10: Size of image

25		**50**		**100**		**200**		**400**		**600**		**800**	
row	col	row	Col	row	col	row	col	Row	col	row	Col	row	col
8096	1024	4048	512	2024	256	1012	128	506	64	253	32	126,5	16

We can see how for pixel size of 600 and 800 meters, the value of local variance can not be representative, since the number of pixels is lower than the recommended minimum. In fact, the land cover greenhouse for a pixel size of 400 meters can not compute local variance since this class disappears. Moreover, the proportion of this land cover in the scene is quite low; table 8 shows the percentage of each class in the selected area.

3) Reviews to the method.

The spatial domain for mapping scale-specific structures of forest vegetation has been object of study in the Peder Klith PhD thesis (Klith Bøcher, 2003). Some aspects such as the size of the window used to calculate the single values of local variance or the way in which the pixels are aggregated to produce larger pixels in the process of constructing the ALV (Average local variance) graph of the method proposed by Woodcock are here criticized.
Although some of the instructions given by Klith could have been applied adapting the function, this would need more time and this is not the main point of the scope of the present study.

In spite of the graph not being as clear as was expected, we can see:
In the cases of land covers grassland, arable land, bare soil mainly in bands 4 and 7, a clear maximum can be distinguished around 100 and 250 m as pixel size.
For the water all bands indicate an optimum pixel size of 800m, obviously large mass of water are being considered, and not small rivers or lakes are detected with this method.
The pixel size more restrictive is 25 m in the land cover built up.
The obtained results showed that a MERIS pixel (300 by 300 m) will contain more than one class, thus the subpixel level should be studied.

4.2.2 Landscape indices

Features of the landscapes were studied by using some indices that show the fragmentation of the studied area. The same image analyzed in the previous section, Landsat TM image from 28th March 2003 have been used here.

Table 11: Features of the landscape

TYPE	CA (ha)	PLAND (%)	NP	LSI
Deciduous forest	31147,87	6,01	13104	164,28
Coniferous forest	56152,62	10,84	11570	120,95
Built-up	61060,12	11,78	37792	248,00
Grassland	226726,12	43,76	22594	209,81
Water	22794,81	4,40	4674	77,62
Arable land	100114,00	19,32	7680	147,22
Bare soil	2019,56	0,39	1475	41,23
Natural vegetation	17800,06	3,43	2569	66,13
Greenhouses	328,56	0,06	433	26,05

Almost half of the studied area is grassland, it appears with 43.75%. Arable land, built up, coniferous and deciduous forest constitute the other 50 % of the landscape. The fact that the percentages in the landscape are distributed between the different classes, except in the case of the grassland, gives an idea of the fragmentation of the landscape. Even more meaningful of this fact is the index LSI and the comparison between the indices CA and PLAND with regard to NP. Although grassland covers more area its LSI is 209.81, indicating that its distributions is scattered and not aggregated in a big patch. Arable land is the second largest class and its LSI is around 150, so its distribution is also disaggregated. The class built-up covers less percentage, 11.78%; however is the class which more patches contain. Thus, it is indicated that the patches

are given out in all the study area and because of that it is the class with the highest value of LSI. In general the value of LSI is high with regard to the surface occupied by each land cover which means that the landscape is quite fragmented. Figure 12 supports this fact.

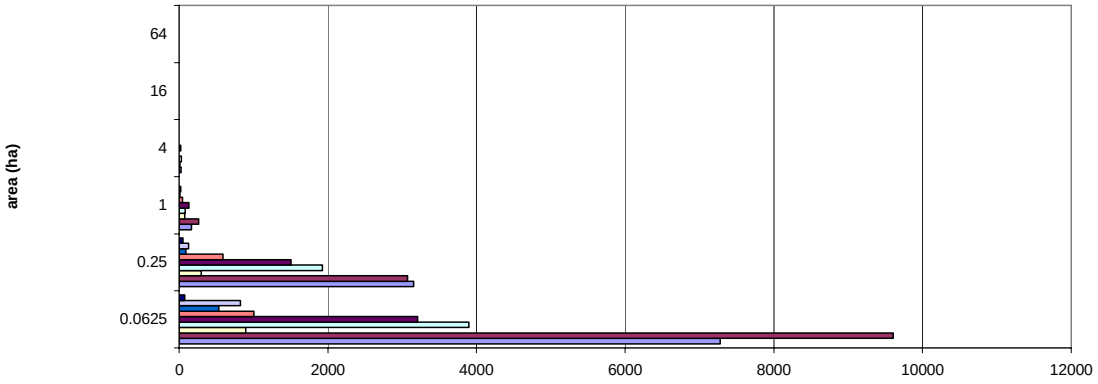

	0.0625	0.25	1	4	16	64
Greenhouses	77	48	4	1	0	0
Natural vegetation	824	125	19	2	1	0
Bare soil	533	93	10	1	1	1
Water	1005	586	45	2	1	1
Deciduous forest	3207	1503	129	22	2	0
Coniferous forest	3900	1924	81	2	1	0
Arableland	895	298	73	30	1	1
Built-up	9608	3071	263	9	2	0
Grassland	7279	3153	165	26	1	1

Number of patches

Figure 12: Histogram of size of patches

Figure 12 represents the number of patches comprised in the landscape of the studied area in The Netherlands.
This histogram represents clearly that the number of patches with an area of 0.0625 ha and 0.25 ha is quite higher than the rest; these areas correspond with a pixel size of 25 and 50 m respectively. And no bars appear in pixel size for 400 and 800 m since only one or two patches appear with that size.
This histogram explains also the necessity of studying subpixel level in the case of MERIS images. The information in a 300 by 300 pixel size is coming from more than one class.
We can observe some differences in the results obtained with both approaches; an example is the land cover water. In the previous method where the local variance is plotted as function of the pixel size, the optimum scale for studying this land cover was 800 m. It is obvious that in this result lakes or small rivers are not being taken into account; however in the histogram it is seen, that there are almost 1000 patches with an area of 0.0625 ha corresponding to water. So, it is other fact that indicates the necessity to search an appropriate scale to make the analysis.

4.3 Conclusions

The most important goal of this chapter was to define the landscape that has been studied. Two approaches have been applied. Both of them show how for studying the different land covers of the landscape, we need to go to a scale around 25 m. MERIS FR has a pixel size of 300 m, thus the information has to be downscaled. Figure 11 and 12 and table 11 support this idea. The class built up is the class more representative. Graph representing built up area in figure 11 shows a maximum local variance for a pixel size of 25 by 25 m. In figure 12 it is this class is which presents a higher number of patches with an area equivalent to this size of pixel. In table 11, it can be observed like built up area covering an 11.8% in the studied area, contains more patches than other classes, indicating the desegregation of this class.

5. Data Fusion. Adaptive window methodology

After demonstrating the necessity of working at MERIS subpixel level, a process of data fusion has been followed. A set of three Landsat TM and six MERIS images were used in this research.

5.1 Methodology

This chapter describes all the steps carried out to test the feasibility of the algorithm proposed by Zhukov et al.(1999), with Landsat and MERIS images.
The method is based on the classification of the high spatial resolution data which succeeds in showing class boundaries clearly, afterward both images are overlayed and the different classes inside of a MERIS pixel can be unmixed.
In the case of Linear Spectral Unmixing, we have the information of the mixed pixel and also the spectral signatures of the individual materials that make up the mixed pixel; the unknown parameter is the percentage in which those materials appear in the scene. This method of Data Fusion presents the same equation, but the unknown parameter is the spectral signature that the endmembers composing the mixed pixel would have in an image with high spectral resolution, in our research MERIS. The percentage of the classes is given by the high spatial resolution image, providing also the position where the different classes in the mixed pixel are found.
The fused image has the spatial information of Landsat and spectral information of MERIS.

Previously to getting the fused images, the next parameters will be optimized:

a. Number of classes in which the high spatial resolution image is classified.
b. Size of window with which the algorithm is applied to the entire image.

Different combinations of these parameters will be tested and the index ERGAS will be used to check the quality of the fused images.
This indicator provides an accurate insight into the overall quality of a fused product and it is considered better than other quality parameters (Wald, 2002). It fulfils three requirements that a good indicator should have:

1. It is independent of units.
2. It is independent of the number of spectral bands under consideration.
3. It is independent of the scales h and l (high and low resolution), making it possible to compare results obtained in different cases, with different resolutions.

After this, a supervised classification of the fused image has resulted in a land cover map. The training areas have been selected based on the LGN5 and the Maximum likelihood classifier has been used to perform the classification. Finally, the error matrix has been used to asses the classification accuracy. Figure 13 shows a schematic overview of the procedure.

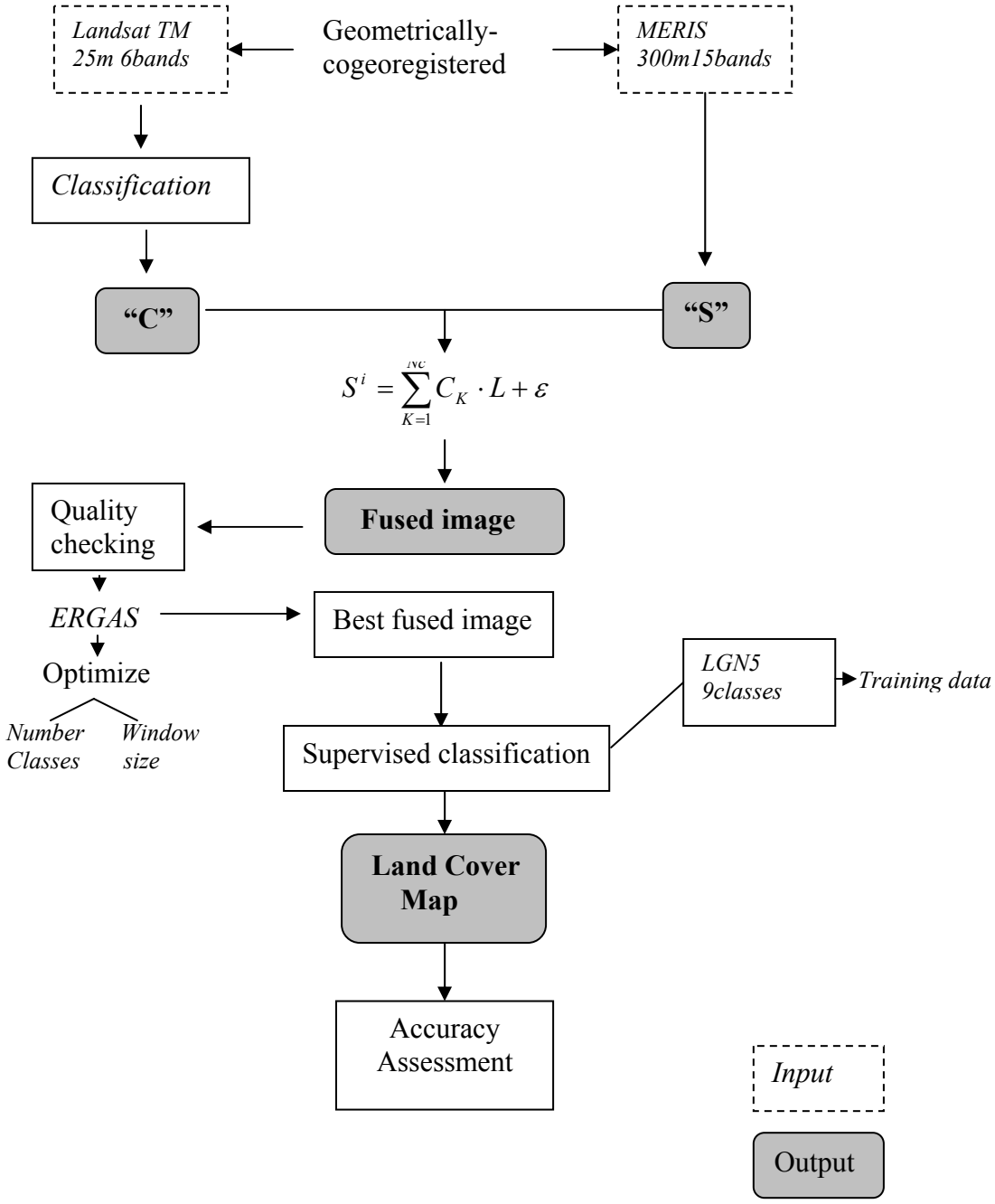

Figure 13: Schematic overview of the Data Fusion analysis

5.1.1 Process of data fusion

The main steps that Zhukov proposed to develop the process of data fusion have been explained in section 2.3. This chapter shows how these steps have been carried out in this research and how the terms of equation 1 have been obtained. Figure 16 shows a schema where appear all the steps for obtaining the fused image.

Proportion of each class *(C)*

The first step in the process of data fusion was to search the proportion of each class in a MERIS pixel. It was explained previously that Zhukov applied the unmix-algorithm by using a sliding window. Each time that the algorithm is solved in a window, we obtain a matrix where the percentages of each class in a MERIS pixel are represented. This matrix will have as many rows as pixels in the MERIS window and as many columns as number of Landsat TM classes. In the case that the MERIS window is 5 by 5 and the Landsat TM image is classified in 10 classes, the matrix fraction will have 25 rows and 10 columns. Therefore, the first line will contain the percentage of each class inside the first MERIS pixel in the window. This matrix is called *"C"* in equation 1.
This process was implemented in MATLAB® and for obtaining the final matrices two initial steps are needed.

Firstly "Propor_maxclass", this function has as inputs: the classified Landsat TM image, the number of classes in which the Landsat images were classified (10, 20, 40, 60 and 80), the sizes of the window that were tested (5, 7, 9, 11 and 13) and ratio *(ratio=TMpixel size/MERISpixel size)*.
Two outputs are obtained; one of them is a matrix of proportions, "*propor"*; this matrix has the size of the MERIS image and it has as many bands as classes appear in the classified Landsat TM images. For instance, in a MERIS image with 422 rows and 82 samples, and a classified Landsat image in 10 classes, the size will be 422 x 82 x 10. In each pixel the fractional percentage of each class in the correspondent MERIS pixel is stored. In the first pixel of the first band appears the fraction of class 1 in the first MERIS pixel. In the first pixel of second band, the fraction of class 2 in the first MERIS pixel appears and so forth. At the end five matrices of proportions are obtained for each Landsat TM date, since the Landsat TM image is classified in 10, 20, 40, 60 and 80 classes (see fig.14).
The other output is the maximum number of classes present in each window; each pixel of the window has the size of a MERIS pixel, because of that we call it a MERIS window.

[propor,maxclasses] = Propor_maxclasses (XC,sw,ratio,I)

Equation 3: Expression of the function Propor_maxclass
(Appendixes I, II, III: Propor_maxclasses and subfunctions).

In a subsequent step this 3D matrix will be converted into a 2D matrix, being this matrix equivalent to the parameter "C" in equation 1. This is a matrix that contains the proportion of each class within a MERIS window.

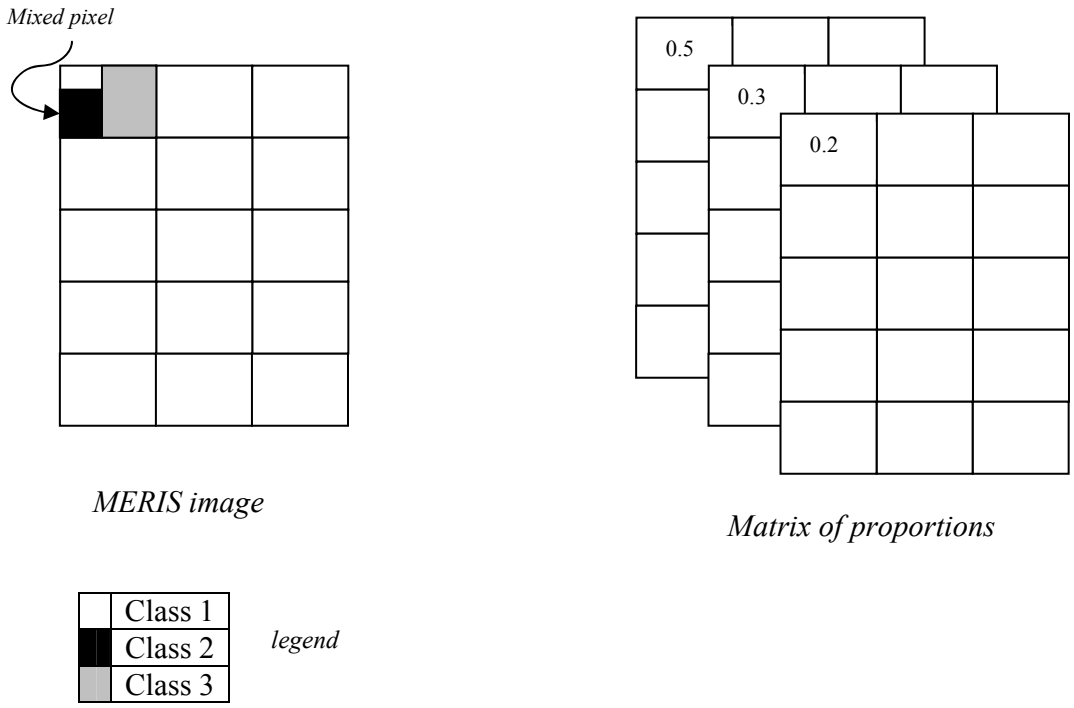

Figure 14: Example of the function *propor_maxclass*. In this case it is supposed a landscape composed by 3 classes.

Radiances MERIS *(S_i)*

The other known parameter in the equation 1, is the Radiances MERIS (S_i). Pixel value is the name assigned to the value of each pixel in each MERIS channel. As it has been explained, the equation 1 is applied to all MERIS pixels in a window. Thus, we obtain as many pixel values as we have pixels in the window. For solving this equation, the radiances in the MERIS window are represented as a column vector with the values of the pixels in the MERIS window.
The MERIS image is crossing by a sliding MERIS window, and each window is transformed to a column.

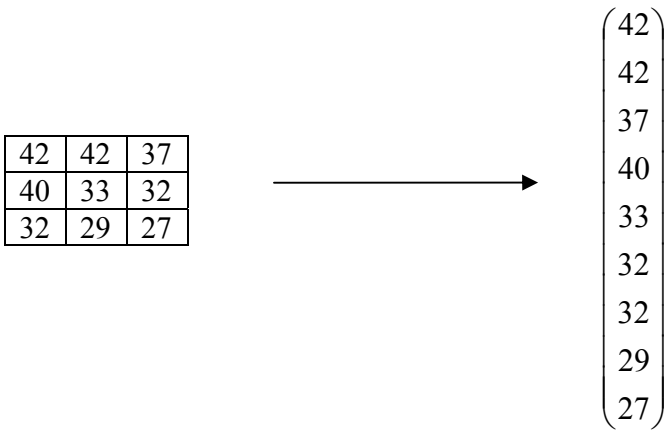

The unknown parameter *(L)*

The only term of the equation 1 that is unknown is *L*. *L,* the endmembers, are the new values of the classes in an image with 25 by 25 m as pixel size and 15 spectral bands.

Data fusion

Once the terms are defined, the equation is solved. The process of image fusion is carried out by Zhukov_MMT, a function implemented in MATLAB ® (Appendix IV). The output of this function is finally the fused image. The main inputs of the fusion function are: the vector with sizes MERIS window (sw); the matrix maxclasses and proportions obtained previously; the vector with different number of classes (XC); the classified Landsat TM image (TM classified) and the method that is going to be used for obtaining the endmembers, the different methods are explained in the next section.

5.1.2 Methods for unmixing

To solve the equation system, two methods have been proposed. These methods search the best solution to solve the equation 3 in different ways. They could be subdivided in:

- Classical methods: They try to minimize the error of the equation 1.
- Current methods: They search the best solution, taking into account ill-posed problems of matrices. These methods are said to apply regularization.

The results of equation 1 were restricted by a lower boundary and an upper boundary. Because we are interested that the rank of the values were 0 to *Lsat*. Table 12 shows the characteristics of these methods.
In appendix VIII some mathematical useful concepts to understand this chapter are defined.

Table 12: Methods for unmixing

Method	***Meaning***	***Characteristic***
Lsqlin	Constrained linear least squares ▪ To solve the least square problem: **Min** $0.5 * \left(\left\| C * L - S \right\|_2^2 \right)$	▪ From MATLAB toolbox optimization ▪ Does not apply regularization
NLCSmoothreg	Non-linear constraint smooth regularization	▪ From Michael Wendlandt ▪ Applies regularization

Some problems were found with the function *NLCSmoothreg*, but with the help of the author we have been able to apply it to solve our equations system.

The syntax of this function is as follows:

gfit = NLCSmoothReg (spectrum, kernel ,lambda ,method ,guess ,tols ,tolg ,maxiter ,as ,lb ,ub)

Equation 4: Expression of NCLSmoothreg; MATLAB®´s application (Wendlandt, 2005)

The inputs of this function are: *spectrum*, in our case this input is the column vector where the values of radiances in each MERIS window are represented; *kernel*, is the matrix with the proportions of each class; the regularization parameter, *lambda*; the method of regularization, in our case Tikhonov; finally *lb* and *ub* meaning lower and upper boundary. The rest of the parameters are established by the author. The output *gfit* are the values of the endmembers.

Michael Wendlandt in his manual used a function of the L-curve proposed by himself. However, using this function the shape of the curve was not similar to a "L", thus it was decided to determine the regularization parameter λ with the application of the L-curve proposed by Per Christian Hansen in Regularization tools (Hansen, 2001).

Another variable that has been included to test the best fused image is "aggregation". Zhukov in one of his articles (Zhukov et al., 1997) once the Landsat image is classified suggests that the small classes of which the total area is less than 0.3 of the TM pixel area are combined with the spectrally closest cluster. This pre-processing has been taken into account in this research, and the fused images coming from classified Landsat TM with classes combined and coming from classified TM image without any post-processing were compared. A threshold of 0.1 was considered. To do this, the application *"**aggregation_fraction**"* has been incorporated into a previous application where the matrix "*C*" was obtained. Doing the aggregation supposes that the vectors linearly dependents in that matrix will decrease consequently the conditional number will also decrease, reducing its ill-posed condition. The conditional number of matrix "C" will be computed to check if a method with regularization should be used.

Therefore, the quality of the fused images will be checked to conclude on the optimal combination of these variables (combinations between methods with and without regularization, with and without aggregation and the parameters previously commented, number of classes and size of windows). Thus, we could give a conclusion about the optimum combination of these variables. The resulting studied cases are combinations of:

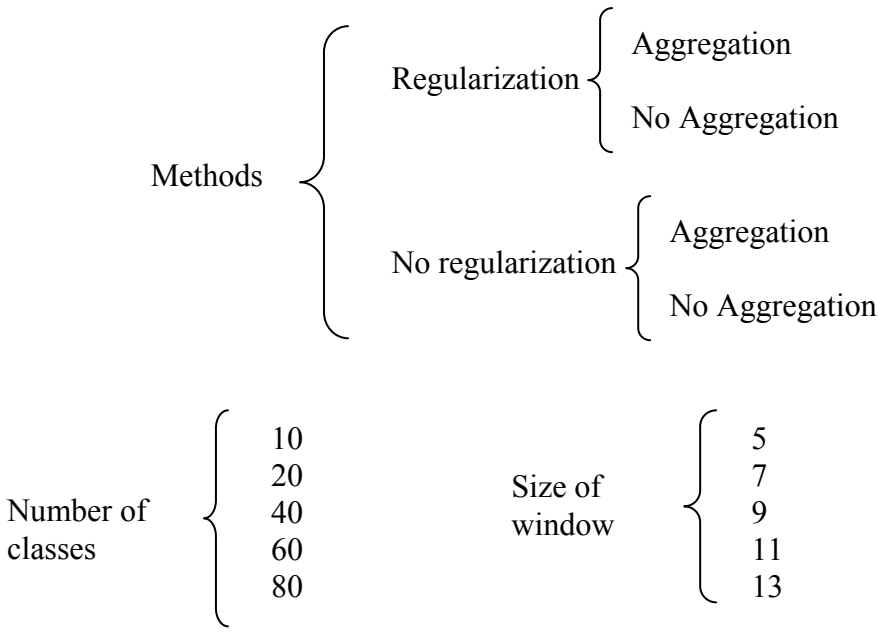

Figure 15: Scheme of all tested combinations

- Lsqlin with aggregation → No regularization and aggregation.
- Lsqlin without aggregation → No regularization and no aggregation.
- NCLSmoothreg with aggregation → Regularization and aggregation.
- NCLSmoothreg without aggregation → Regularization and no aggregation

The last step for getting the fused images once the equation is solved in the MERIS window is made with another application implemented in MATLAB® called ***Recomposed_fused_col***. This function arranges the fused pixels that are going to be obtained when the equation 1 is applied in the MERIS window in each band. Finally, when the 15 layers are fused, they are stacked by means of an application made with DELPHI, ***Layerstack_stream.exe***.

Running the program of Zhukov needs a processing long time. For this reason, to choose the method to apply to all images and also to optimize the number of classes in the TM image and the window size to solve the unmixing was made using one TM image (28th March) and one MERIS image (18th February). With the decision made from these results, the rest of the images will be fused.

What is Lsat?

Lsat is the maximum value of radiance that a valid MERIS detector can reach for a given wavelength. A MERIS pixel may be affected by phenomena outside the range of useful measurements; for instance, sun light, cloud, bright land or snow/ice. When this has happened, the invalid value should be replaced by a good estimate (www2).
Table 13 shows the values of Lsat per MERIS band; these values have been obtained from the handbook of MERIS in the web of ESA. Once these values were applied, the quality of some bands in the fused images turns out very poor. The reason is that the used values of Lsat correspond to a tuning of MERIS optimised for Ocean observation-MERIS´s primary mission. Claims from the land community that the InfraRed bands are

of great scientific interest for land targets lead the Science Advisory Group to change the MERIS settings significantly in order to accommodate for typical land targets without saturation. The actual values of the saturation radiance Lsat were derived from the measured calibration gains and the various parameters of the instrumental effects correction. These values appear in the third column of table 13.
Although these values could solve the inaccuracy with these bands, the problem was detected once the results had been obtained; because of that the values of Lsat for ocean applications were used. Nevertheless, an improvement was tried. The program for doing the data fusion was modified, and the process of data fusion was repeated for the case that we considered providing the best results. The change in the program was to assign the highest value that the endmembers values can take to the maximum value per MERIS band instead of the values of Lsat found in the web of *ESA*.

Table 13: Lsat values for ocean and land applications

Spectral band ID	Lsat (ocean) ($mW/m^2/sr/nm$)	Lsat (land) ($mW/m^2/sr/nm$)
B1	251.5	615.865
B2	268.3	689.226
B3	260.8	752.982
B4	240.1	695.869
B5	232.7	606.407
B6	214.2	532.228
B7	240.3	445.125
B8	199.2	450.968
B9	39.0	410.083
B10	383	563.201
B11	377	576.742
B12	30.0	236.120
B13	186.3	231.032
B14	26.0	369.742
B15	124.4	352.986

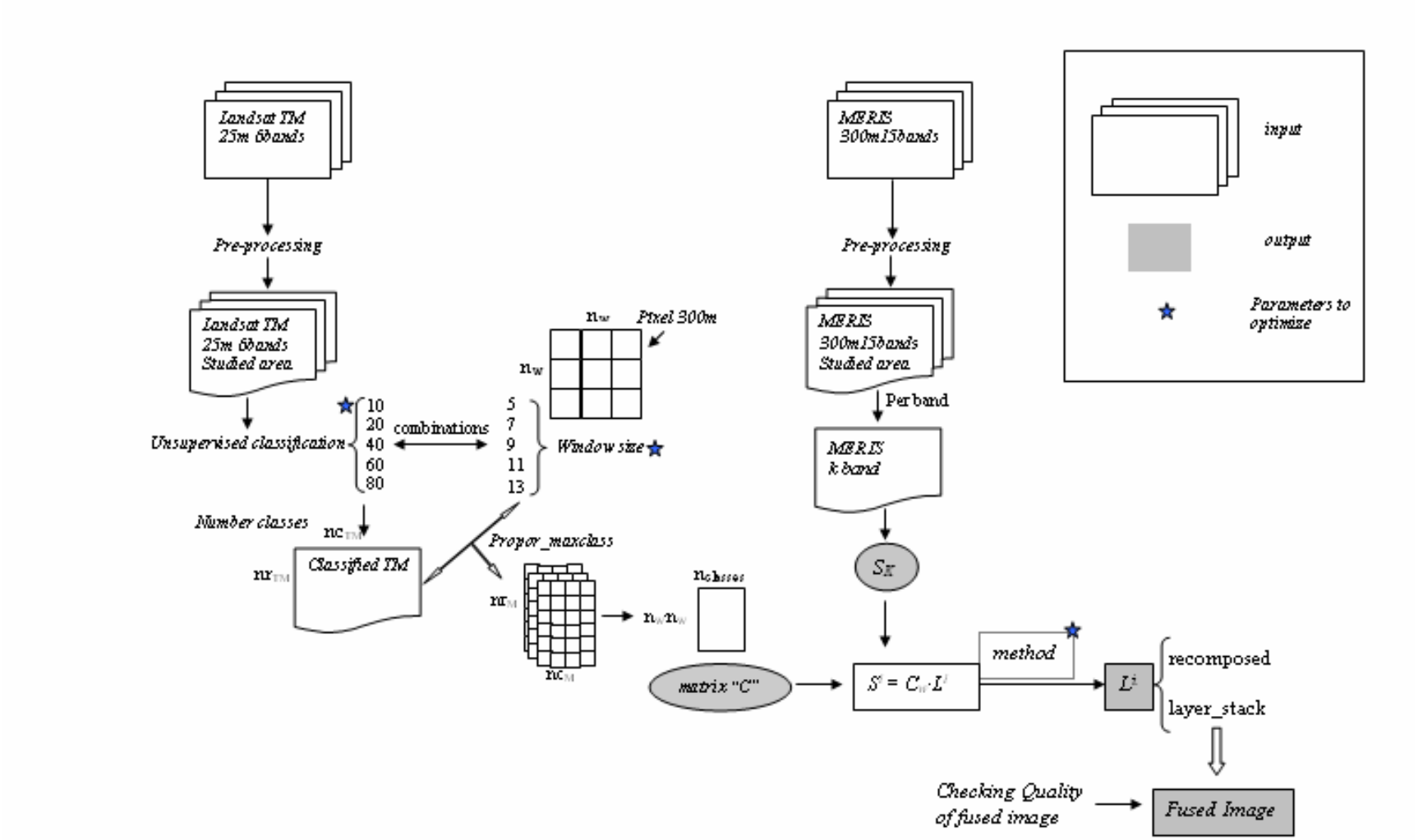

Figure 16: Shematic overview of the process of data fusion

5.1.3 Quality of the fused images

To validate the proposed method a quantitative analysis of the fused images was performed. Fused images should be as close as possible to reality and should simulate what would be observed by a sensor having the same features as MERIS but the highest spatial resolution (Wald, 2002). The increase in the use of different methods of data fusion in the last years has made that many remote sensing researchers worry about the quality of these fused images (Acerbi-Junior et al., 2005b; Beauchemin et al., ; Garguet-Duport et al., 1996; Thomas and Wald, 2005). Many of them agree that to establish criteria to assess the quality of the fused images is not a simple task since the quality assessment relies on several factors; for instance the type of landscape and the resolution are decisive on the accuracy in the process of fusion (Thomas and Wald, 2005). Some of the parameters proposed in the literature have been used to check the quality of our images.
First of all, the resampling of the fused images down to the low resolution has been made, and the MERIS image was taken as reference. Any synthetic image once degraded to its original resolution, should be as identical as possible to the original image.
Comparison of both images has been based on their spectral characteristic and was performed visually and quantitatively using statistical parameters and one quantitative index.
The fused images were downscaled, using the mean, to the resolution of the MERIS images.
In order to estimate the global spectral quality of the fused images we have used the ERGAS index. The ERGAS index is a relative dimensionless global error index of the fusion process. The error ERGAS exhibits a strong tendency to decrease as the quality increases. Thus, it is a good indicator of the quality and behaves correctly whatever the number of bands is because it uses for each band the RMSE relative to the mean of the band (Wald, 2002).

The expression of this index is:

$$ERGAS = 100\frac{h}{l}\sqrt{\frac{1}{N}\sum_{i=1}^{N}\left(RMSE^2(B_i)/M_i^2\right)}$$

Equation 5: Formula of ERGAS index

$$RMSE(B_i) = \sqrt{\frac{1}{NP}\sum_{k=1}^{NP}\left(B_i(k) - B_i^*(k)\right)^2}$$

Equation 6: Formula of RMSE

Where:

h, is the resolution of the TM images (h=25 m).
l, is the resolution of MERIS images (l=300 m).
N, is the number of spectral bands (B_i) involved in the fusion (N=15).

M, is the mean value of each spectral band of the MERIS image.
RMSE, root mean square error.
NP, is the number of pixels.
B^*, is the band of the downscaled fused image.

To optimize the number of classes, the size of window and to decide which methods for solving the equation system provide the most accurate fused image, the ERGAS index was computed for all the obtained images.
An optimum solution was not clearly found, thus we chose the combinations that had given the best three values of ERGAS, and the fusion for all the dates was made those combinations.

Then, the mean, the standard deviation, the correlation coefficient and root mean square error (RMSE) were computed for the MERIS and the downscaled fused images. These parameters allow us to determine the difference in spectral information between each band of the fused image and the original image (González-Audícana et al., 2005).

5.1.4 Classification

Once we obtained the final fused image, the classification of them was performed by using maximum likelihood algorithm, as it is the most popular for classification of remote sensing imagery (Carvalho et al., 2004). This method is based on the assumption that the frequency distribution of the class membership can be approximated by the multivariate normal probability distribution. The probability P(x) that a pixel vector **x** of *p* elements is a member of class *i* is given by the multivariate normal density distribution (Mather, 2004):

$$P(x) = 2\pi^{-0.5p}\left|S_i\right|^{-0.5}\exp\left[-0.5\left(y`S^{-1}y\right)\right]$$

Where:

P(x); likelihood of x belonging to class i
$|.|$ denotes the determinant of the specified matrix
S_i is the sample variance-covariance matrix for the class i
$y = x - \overline{x_i}$
$\overline{x_i}$ is the multivariate mean of class *I.*

Figure 17 shows the concept of the maximum likelihood method.

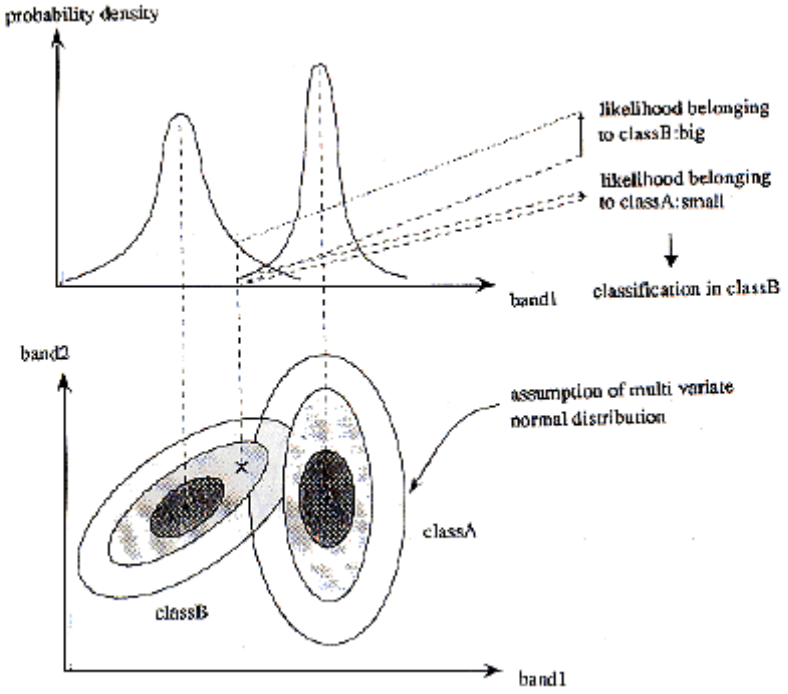

Figure 17: Maximum likelihood example

To apply this algorithm it is necessary to have some training areas in the fused images, regions belonging to the different classes. This is data sampling.

Data sampling

Training data is required to classify the fused images. Taking as ground truth image the LGN5 aggregated to nine classes, some regions were marked of each class in the fused image. For that, LGN5 should contain the 9 classes in the selected studied area. However some classes appear in very low percentage, i.e. greenhouses and bare soil. The number of pixels that constitutes these training areas is shown in table 14. In table 15 the percentages of each class in the studied area are listed.

Table 14: Identified pixels per aggregated land use class constituting the training areas

Land use	***Number of pixels***
Water	2415
Built up	270
Arable land	2027
Grassland	1076
Bare soil	467
Greenhouses	13
Natural vegetation	289
Deciduous forest	76
Coniferous forest	1316

Table 15: Percentage of each class in the studied area for the process of data fusion

Land use	***%***
Water	4.27
Built up	14.47
Arable land	22.69
Grassland	35.42
Bare soil	0.48
Greenhouses	0.07
Natural Vegetation	3.01
Deciduous forest	6.43
Coniferous forest	13.16

(Table 11 and 15 show different perecentages since table 11 is refered to LGN4 and table15 to LGN5)

Accuracy matrix

Once the classification has been carried out we determined the degree of accuracy in the end product. The most commonly used method of representing the degree of accuracy of a classification is to build a *k x k* confusion matrix. The elements of the rows *i* of this matrix give the number of pixels which the operator has identified as being members of class *i* that have been allocated to class 1 to *k* by the classification procedure. Element *i* of row *i* (the *i*th diagonal element) contains the number of pixels identified by the operator as belonging to class *i* that have been correctly labeled by the classifier. The other elements of row *i* give the number and distribution of pixels that have been incorrectly labeled. The classification accuracy for class *i* is therefore the number of pixels in cell *i* divided by the total number of pixels identified by the operator from ground data as being class *i* pixels (Mather, 2004). Overall accuracy uses only the main diagonal elements of the matrix; it does not take into account the proportion agreement between data sets that is due to chance alone and because of this it tends to overestimate classification accuracy (Congalton and Mead, 1983). In order to compensate for this, the index Kappa or KHAT is used.
This index ranges between 0 and 1 and expresses the proportionate reduction error achieved by a classifier as compared with the error of a completely random classifier (Lillesand and Keifer, 2000). The formula for computing the KHAT is:

$$\hat{K} = \frac{\text{Overall Classification Accuracy} - \text{Expected Classification Accuracy}}{1 - \text{Expected Classification Accuracy}}$$

Equation 7: Formula for computing Kappa (Verbyla, 1995)

5.2. Results

5.2.1 Conditional Number

First of all, the conditional number of the matrices "C" was checked to observe if it would be advisable to apply regularization to solve the equations system.

Two histograms showing the distribution of the conditional number in the classified Landsat TM image from 10th July 2003 for both cases, with and without aggregation, are presented in the figures 18 and 19. These values correspond to the conditional numbers of a matrix "C" obtained from a classified TM image in 20 classes and use of a sliding window of 7 by 7 pixels.
Since we are working with a sliding window, as many matrices "*C*" as number of pixels in the MERIS images are created. . The original size of the MERIS image is 422 rows by 82 samples. When columns and rows affected by effect of the frame of zeros are removed, MERIS image is 416 rows by 76 columns. Thus, 31616 matrices are obtained.

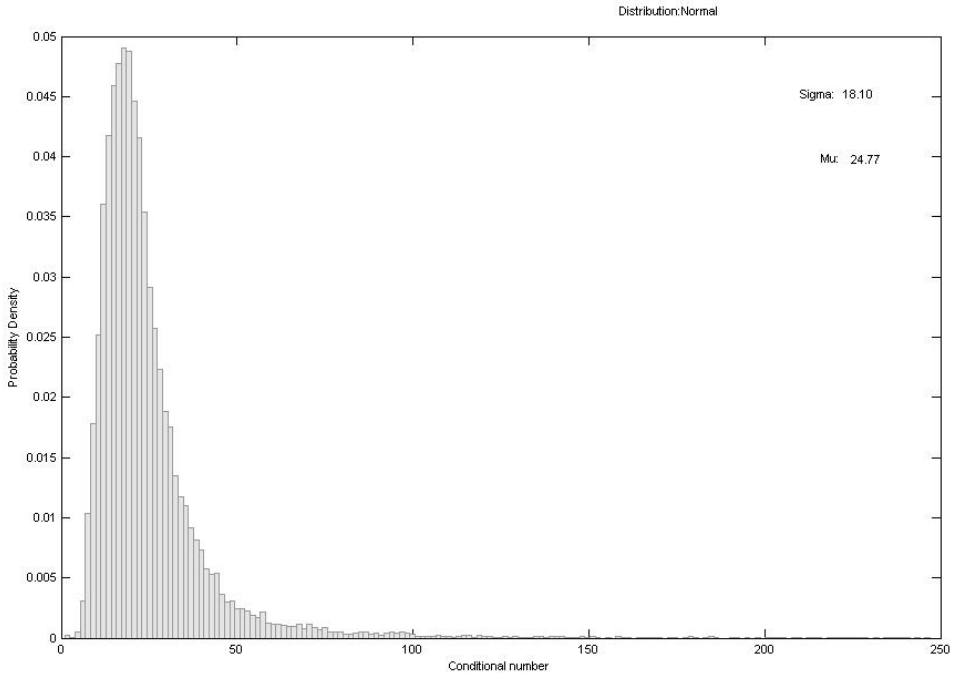

Figure 18: Conditional number with aggregation (tm5_10072003)
(axis X: Conditional Number; axis Y: Probability density)

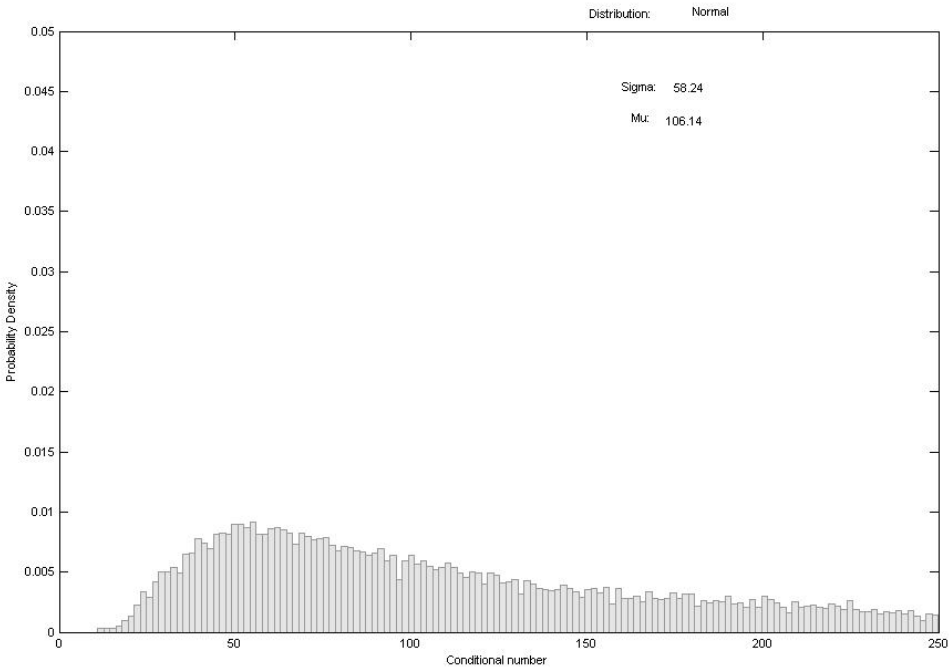

Figure 19: Conditional number without aggregation (tm5_10072003) (axis X: Conditional Number; axis Y: probability density)

The histograms only represent conditional number in a rank from 0 till 250. The highest value was infinite and once the infinite was removed, the values continue being very high (table 16).

Table 16: Data of Conditional numbers

	Fractions_agg	Fractions_noagg
Max	Inf	Inf
Num.Elem whose CN<Inf	31353	31605
Max (once removed Inf)	6,2013e+046	3,1977e+140
Mean(once removed Inf)	1,9779e+042	1,0118e+136

As it is indicated in table 16, the maximum conditional number is infinite. It can be observed that there are more infinites in aggregated matrices than in non aggregated. When the infinite values are eliminated, the number of fractions non aggregated whose conditional number is lower than infinite is higher than in the case of the fractions aggregated. This fact can happen when there are areas composed in majority by the same class. If the classes that appear in smaller proportion are combined, all the neighbors' pixels in that area will present the same vector of proportions. Then the matrix will be ill-posed and will increase the conditional number.
However, when the infinite values are removed, the maximum conditional number is smaller in aggregated matrices than in non aggregated. Also in the histograms, which show the lowest values of the conditional number, it can be seen how they are smaller once the matrices have been aggregated. The peak represents the conditional number that appears more frequently; in aggregated matrices is 18.1 and in the case of non-

aggregated matrices is 58.24. The values of the conditional number in non aggregated matrices seem to be distributed along all the values; they do not appear with high frequency around one value.
It can be concluded that the aggregation will improve the ill-posed condition of the matrices, and a better solution should be obtained. However, the conditional numbers continue being very high, consequently a method applying regularization should be used. Nevertheless both methods, with and without regularization, and also, with and without aggregation of the matrices, were tried for the Landsat TM image from 28th March and the MERIS image from 18th February 2003. This was done only for those dates, because to run the program to fuse the images takes a long time.

5.2.2 Quality of the fused images using upper boundary Lsat Ocean

Once all combinations were computed to fuse the Landsat TM from 28th March and MERIS from 18th February, the ERGAS index was computed as first approximation to decide the best way to fuse the images (table 18 and 19). The shadow cells are the cases in which there are a larger number of classes in the window than equations. Table 17 shows the number of classes per window for the cases in which it is not possible to obtain a solution.

Table 17: Cases with no solution

		Number of classes		
Window size	***Number of equations***	**40**	**60**	**80**
5	**25**	40	60	79
7	**49**	40 (possible)	60	79

Table 18: ERGAS without applying regularization *(Lsqlin)*

	Number of classes in Landsat TM image				
Window size	**10**	**20**	**40**	**60**	**80**
5	3.247	2.970			
	3.458	3.530			
7	3.242	2.963	3.105		
	3.452	3.525	3.953		
9	3.238	3.571	3.380	3.214	3.089
	3.447	3.524	3.952	4.701	*Error***
11	3.237	3.570	3.395	3.432	3.319
	3.446	3.902	4	4.503	5.945
13	3.234	3.834	3.699	3.581	3.482
	3.445	3.901	4.002	4.507	5.964

Table 19: ERGAS applying regularization *(NCLSmoothreg)*

	Number of classes in Landsat TM image				
Window size	**10**	**20**	**40**	**60**	**80**
5	3.48	3.259			
	3.846	*Error***			
7	3.471	3.243	3.053		
	3.835	3.902	4.076		
9	**	3.234	3.048	**	**
	3.829	3.893	4.070	6.071	10.014
11	3.973	3.229	3.719	**	**
	3.823	4.027	4.068	4.523	5.884
13	3.975	3.224	3.718	**	**
	3.821	4.025	4.102	4.528	5.901

No aggregation	The matrix fraction in not aggregated
Aggregation	The matrix fraction is aggregated

***The incomplete data have mistakes while the program was running in the case of the errors or problem in the time for computing a band. It was decided not to continue with the fusion, because this was requiring almost eight hours per fused band.*

An ERGAS greater than 3 corresponds to fused products of low quality, while an ERGAS lower than three denotes a product of satisfactory quality or better (Aiazzi et al., 2004).
As we can see, the values obtained do not follow a pattern; it is difficult to conclude which is the optimum number of classes and the window size to obtain the fused image. Even it is difficult to decide the method, since it has turned out that "lsqlin" provides the best results, which is the method that does not apply regularization. This fact was unexpected; a method applying regularization should give better results than the other since, like it was explained before, the purpose of regularization is to stabilize the ill-posed problem and to single out a stable solution. Neither the aggregation has improved the results.
In the case of the aggregation, the problem could be the threshold. We have checked a threshold of 0.1, when the proportion of a class in a MERIS pixel is lower than the threshold, a combination of this class with the rest of the class in the pixels was done. This threshold should depend on the number of classes in which the Landsat TM image is classified. For instance, the same threshold for a classified image in 10 classes will be lower than a classified image in 80 classes, since with the same constraint many classes can be lost in this second image.

Since a clear conclusion could not be obtained, each data set of images was fused with the method, window size and number of classes that had given the smallest values of ERGAS. The best combinations were:

Method	*Number of classes*	*Size of window*
No regularization, noaggregation → lsqlin_noagg	20	7
	80	9
Regularization, no aggregation→ NLCSmoothreg_noagg	40	9

Once the fusion was made, the ERGAS index was computed and it showed values higher than 3 for the rest of the data set of images. Table 20 presents these results.

Table 20: ERGAS for every date set of images

		Lsqlin_noagg		**NLCSmooth_noagg**
TM dates	**MERIS dates**	**class20 ws7**	**class80 ws9**	**class40 ws9**
28.03.03	18.02.03	3.092	2.860	3.306
	16.04.03	7.583	7.451	7.696
10.07.03	06.06.03	9.395	9.333	9.458
	14.07.03	8.892	8.712	8.964
11.08.03	06.08.03	8.193	8.113	8.229
	09.08.03	8.217	8.103	8.260

The values for the MERIS image from 18th February are a bit different to tables 18 and 19 because a mistake was detected after the fusion of all images. The values of the MERIS image had lost the decimals to be multiplied by the gains to transform the values in radiance. This error was corrected, and the final images have not this failure.

This index fails in measuring the spectral distortion, and it does not consider the correlation coefficient (Aiazzi et al., 2004), thus some statistical parameters were computed, in order to check if the ERGAS values were being distorted.

Figure 20 shows these parameters:

*Graph 20.a. Bias. The bias is computed like the difference between the mean of fused image resampled to MERIS resolution and the mean of the original MERIS images. The ideal is bias 0.

*Graph 20.b. Correlation coefficient. This measure indicates how well trends in the values from fused image resampled follow the trends of the real values form MERIS image. It is number between 0 and 1. A perfect fit gives a coefficient of 1.

*Graph 20.c. Standard deviation. The deviation with regard to the mean is measured. In this graph the values from MERIS image are represented with (*) and the values from fused image resampled with (·), each color corresponds to a date. Thus there are two graphs of the same color for each date. The quality is better when both graphs are similar.

*Graph 20.d and e. RMSE absolute and normalized

$$RMSEnormalized = \frac{RMSE}{meanMERIS}$$

Equation 8: RMSE normalized

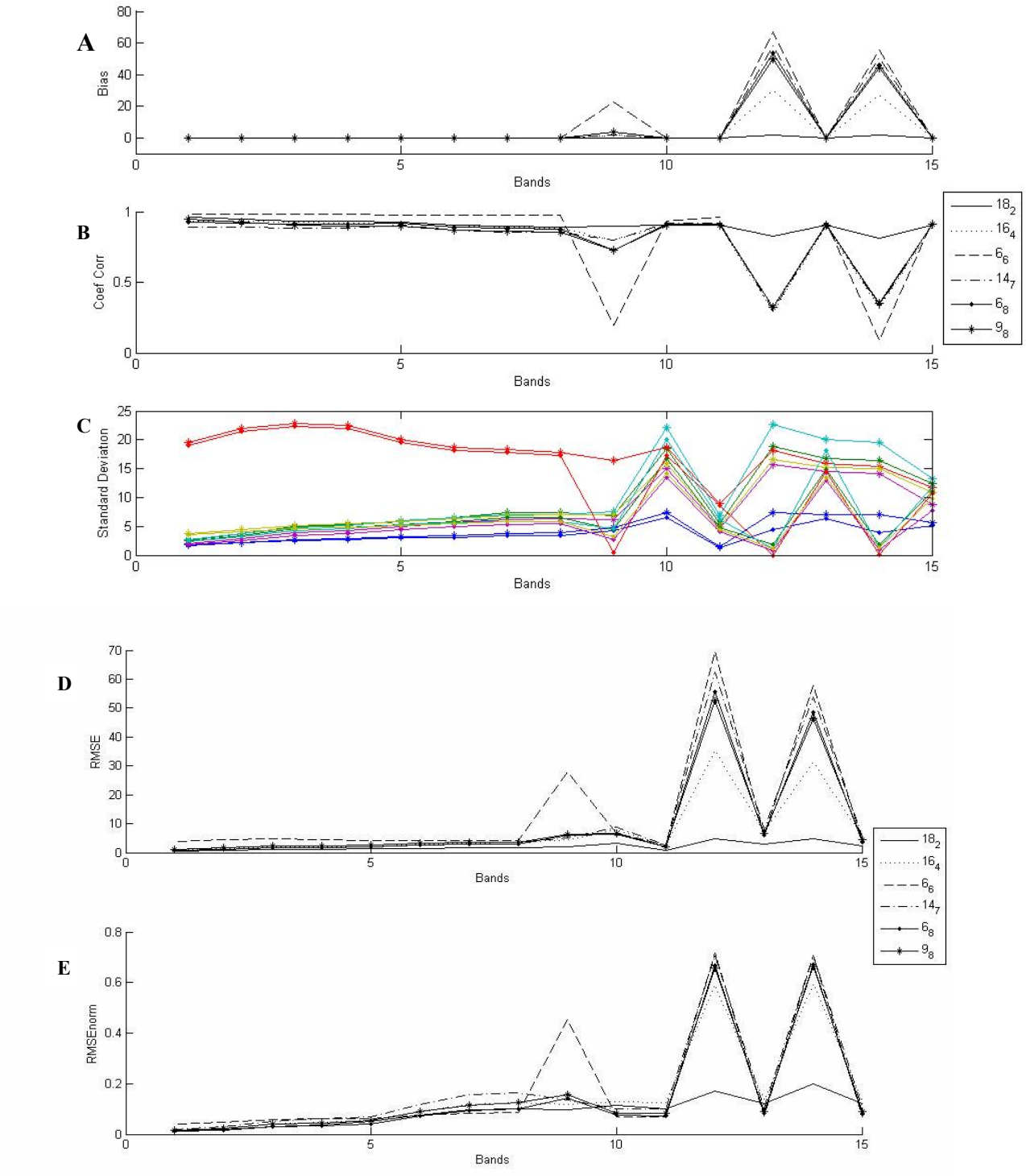

Figure 20: a) Bias; b) Correlation coefficient; c) Standard deviation; d)RMSEabsolute; e)RMSEnormalized. Images from Lsqlin_noaggClass20ws7

The five statistical parameters indicate a poor quality in the bands 9, 12 and 14. The best values in these bands correspond to the fused image from 18th February (MERIS) and 28th March (TM), for this reason the ERGAS values were better. The values of ERGAS without taking into account these bands were computed and they improved remarkably.

Table 21: ERGAS for 15 and 12 bands

		Lsqlin_noagg				**NLCSmooth_noagg**	
TM dates	**MERIS dates**	**class20 ws7**		**class80 ws9**		**class40 ws9**	
		ERGAS 15bands	*ERGAS 12bands*	*ERGAS 15bands*	*ERGAS 12bands*	*ERGAS 15bands*	*ERGAS 12bands*
28.03.03	18.02.03	3.092	2.403	2.860	2.042	3.306	2.678
	16.04.03	7.583	2.824	7.451	2.464	7.696	3.105
10.07.03	06.06.03	9.395	1.935	9.333	1.593	9.459	2.209
	14.07.03	8.892	2.881	8.712	2.280	8.964	3.094
11.08.03	06.08.03	8.193	1.904	8.113	1.543	8.229	2.058
	09.08.03	8.217	2.282	8.103	1.847	8.260	2.439

Table 21 shows values quite similar between the different methods. To decide finally the best fused images, visual interpretation and comparisons between the spectral profiles of the classes was made in the different images. A method without regularization was decided to provide better results.

Figure 21 shows the results for fused images from MERIS image 14 July 2003 and Landsat TM image 10 July 2003 and from MERIS image 28 March 2003 and Landsat TM image 16 April 2003. To the left of the array appear the original MERIS (first) and Landsat TM (second) images and to the right the three fused images obtained by the three chosen combinations.
We can see how the images "3" present a dark frame corresponding to the padding made for being able to compute the equations of unmixing also in the pixels in the border. Also these dark pixels appear in some places in the images, they are indicated with a red ellipse and it is clearer in the figure 22. This last fact made us to decide for the method without regularization.
Between the other images there are no considerable differences. The spectral profiles of some classes were compared (figure 23), but they were not decisive about the best classification and window size.

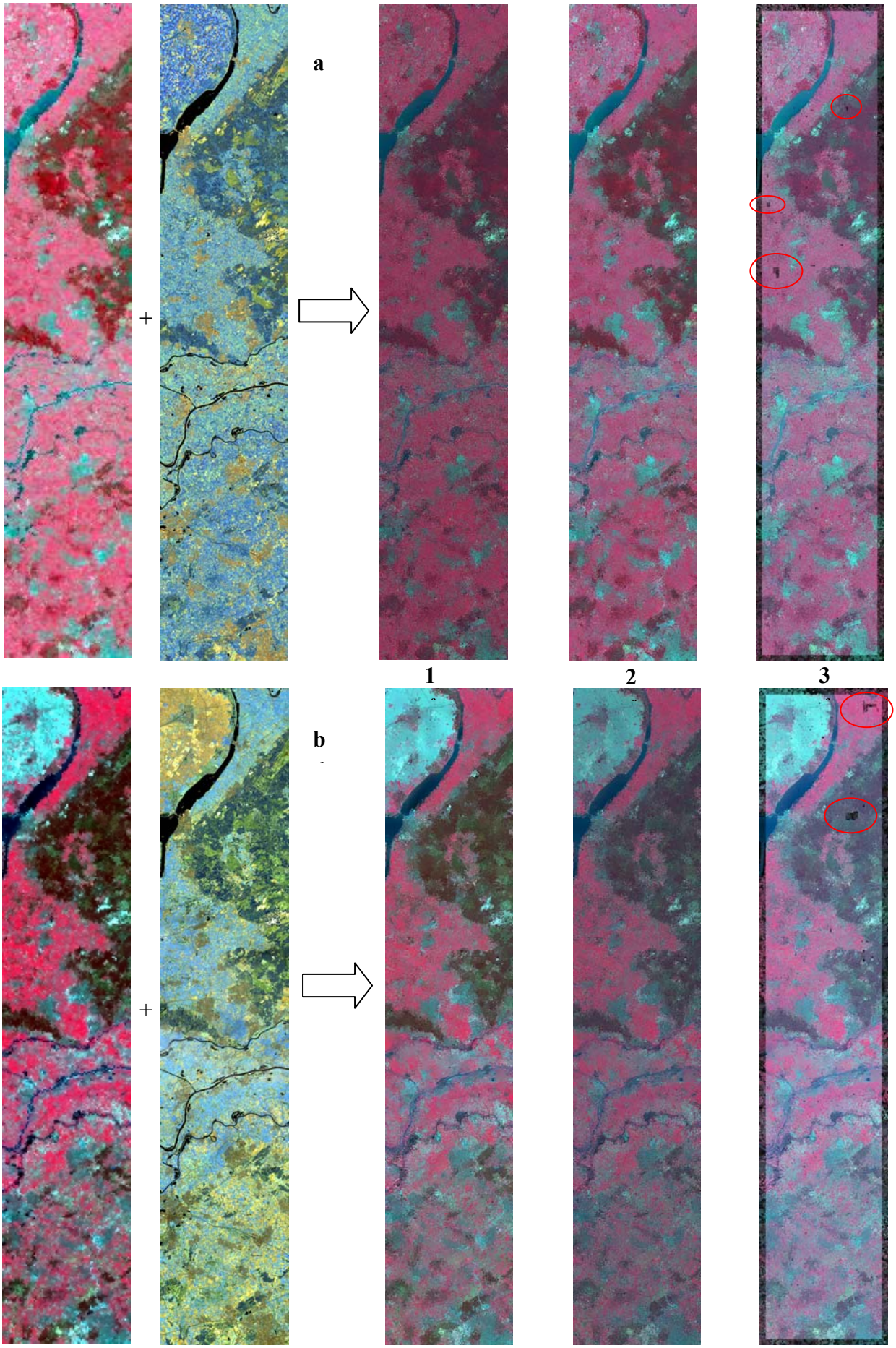

Figure 21: Fused image from (a) MERIS14july+TM10july (b) MERIS 16April+TM 28March→Fused images (1) lsqlin_noagg_20_7 (2) lsqlin_noagg_80_9 (3) NLCSmoothreg_40_9

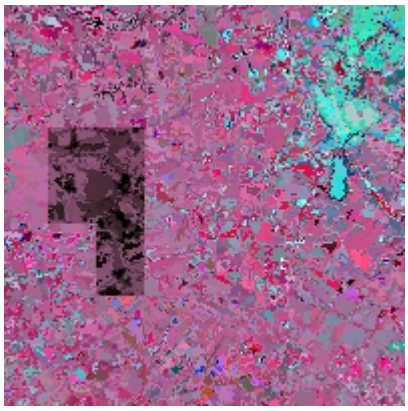

Figure 22: Zoom of dark pixels

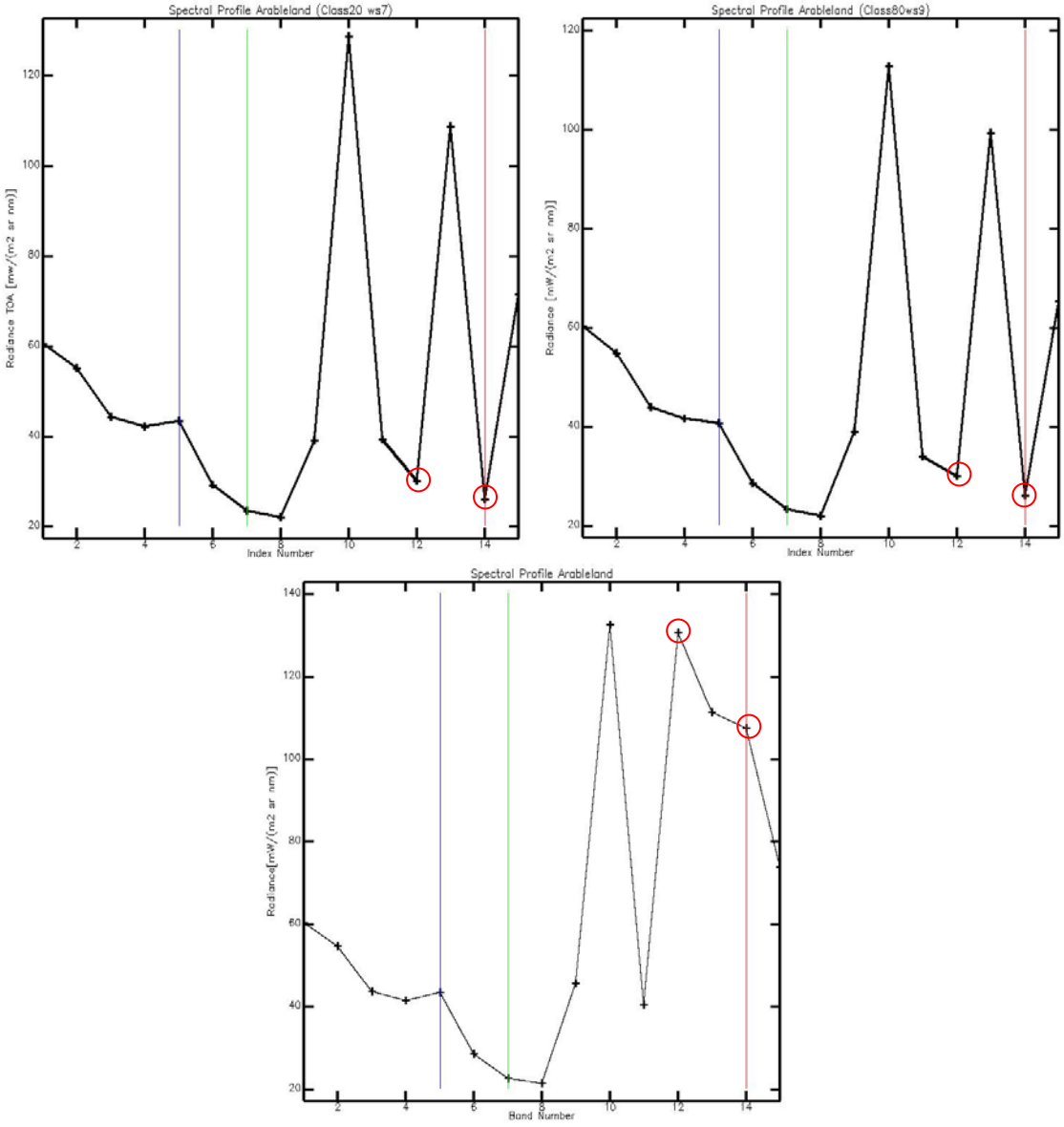

Figure 23: Spectral profiles of class arable land (1) Upper left; fused image class20 (2) Upper right; fused image class 80 (3) Middle; Original MERIS (X: Bands; Y: Radiance(mW/m2 sr nm))

In figure 23, if band per band is checked, we can see the resemblance between the spectral profiles from fused images and from original MERIS image. All the bands show the same spectral signature as the original; only difference is found in the defaulty bands 12 and 14 (red circle). The rest of the classes present the same conclusions, but less for the land cover water, where the spectral profile of fused images as original MERIS image is very similar for all bands.

Finally, the fused image obtained with a method not applying regularization, the Landsat TM image classified in 20 classes and a window size of 7 by 7, was chosen for making the supervised classification and later to obtain a map of land cover for The Netherlands.

Classification

Maximum likelihood was the algorithm used to perform the classification of the image. First, training areas distributed over the 9 classes were selected based on the LGN5, constituting the regions of interest. The corresponding number of 25 by 25 m pixels constituting these areas and subsequently to derive the spectral signatures of the different endmembers is listed in table 14.

The spectral signature of the endmembers for each of the nine classes was derived and later compared with the spectral signature obtained in a research carried out by Zurita Milla et al. (2005). In this research the spectral signatures of the nine classes were made from the image of 14th July, using locations identified in the LGN4, the spectral signatures from this study are belonging to the image of 14th July also (figure 24).
In the plot obtained from the classified fused image, it can be observed how the spectral signature of the greenhouses appears quite mixed with the rest of the classes making this class with difficulty recognizable. Other difference between these two plots is found in the problematic mentioned bands. They present low values of radiance, like the absorbance peaks. These bands seem to be quite important to distinguish between land uses, like arable land, grassland and deciduous forest whose spectral signature in the visible part of the spectrum presents strong resemblance and they are better distinguished in that part of the Near Infrared.
The classification results obtained are summarized in table 22.

Table 22: Overall accuracy and kappa coefficient

	Overall accuracy	**Kappa**
18 February	40.82%	0,3077
16 April	41.23%	0,3355
06 June	40.73%	0,2850
14 July	42.36%	0,3005
06 August	38,25%	0,1706
09 August	36,13%	0,1008

These percentages have been estimated without considering the land cover greenhouses. Greenhouses appear in quite a low percentage in this area of The Netherlands, only 0.071 % (table15) and also quite distributed in the scene. It is possible that this

percentage was not enough to estimate the spectral signature of this land cover, and the spectral signature that we are obtaining does not belong to the pure endmember greenhouse, thus a bad classification of this land cover is obtained and because of that it is confused with the rest of the classes. If greenhouses were taken into account in the classification, many pixels were associated to this class. For this reason it was decided not to include them in the classification. The classification process depends on the spectral information and any error in the synthesis of the spectral content of the fused image will result in classification errors (Acerbi-Junior et al., 2005a)

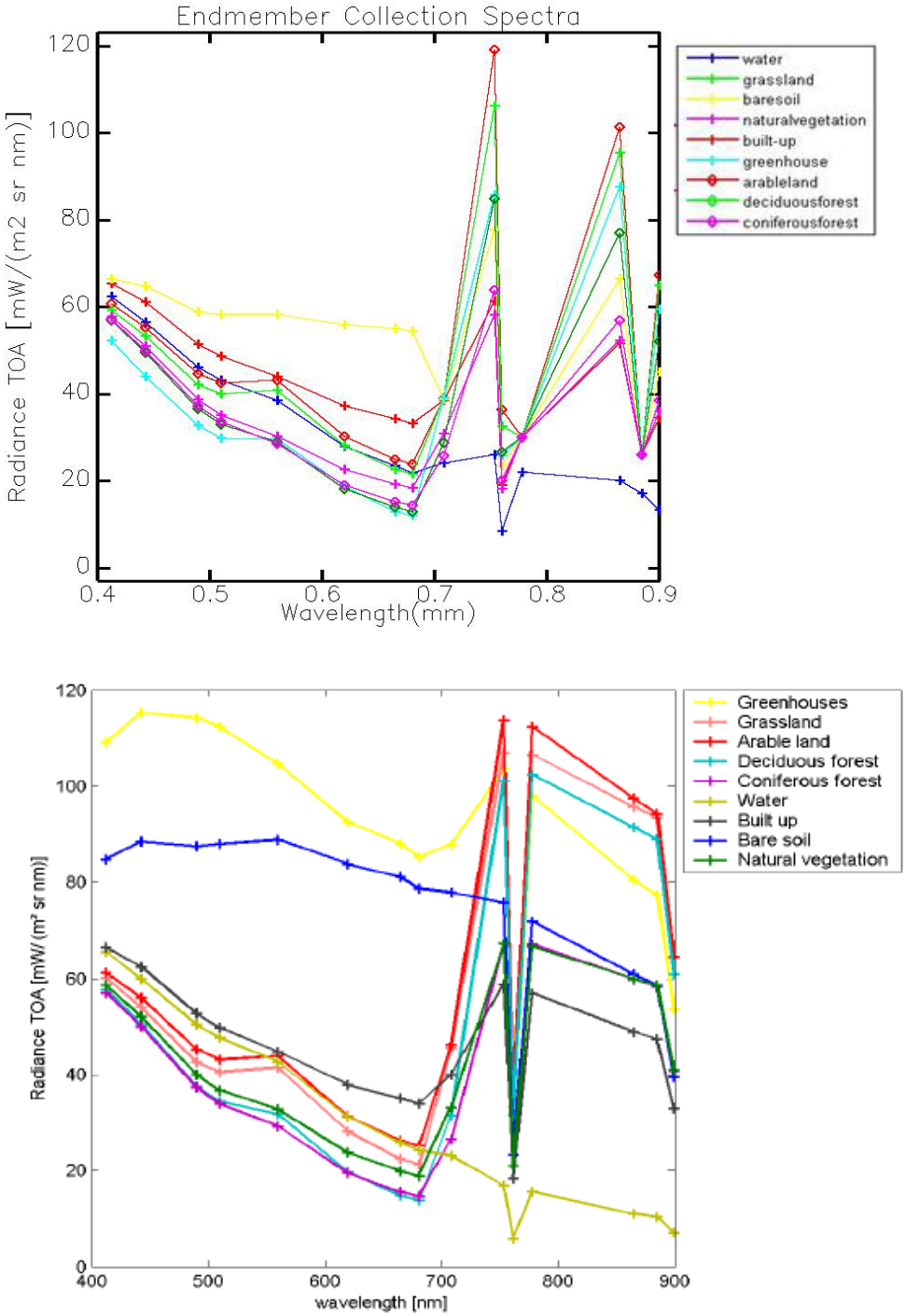

Figure 24: Endmember for the 14th July 2003. Up; derived from this study. Down; (Zurita Milla et al., 2005)

Once that the data were studied, it was concluded that the problem was the values of Lsat obtained in ESA web (table 13, Lsat ocean).
The Lsat for these problematic bands is:

Bands	Lsat ($mW/m^2/sr/nm$)
9	39.0
12	30.0
14	26.0

And the histogram obtained with the radiance values for bands 9 and 12 are:

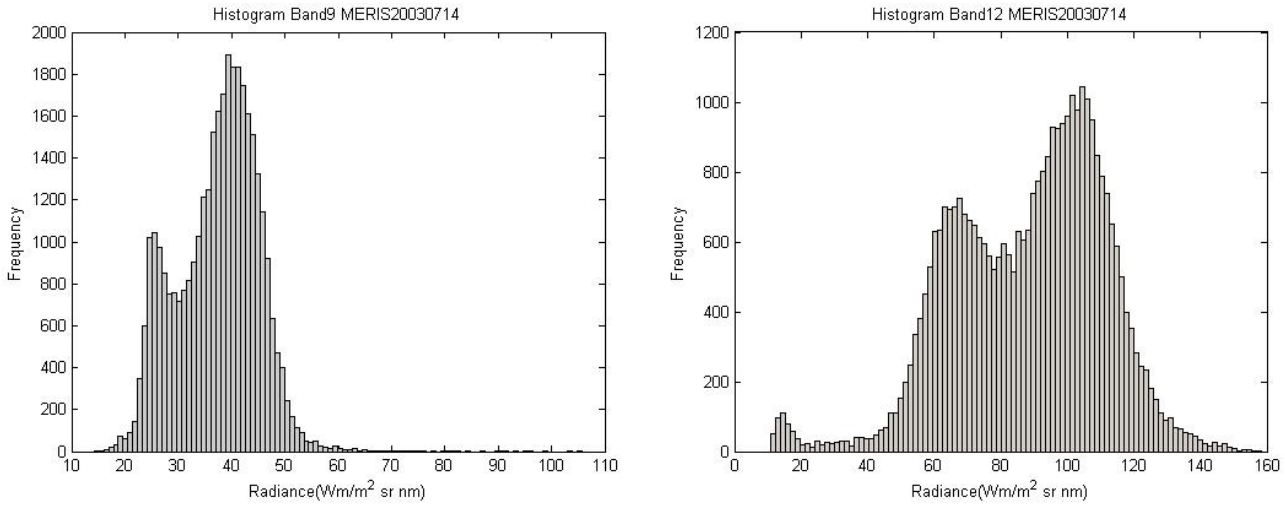

Figure 25: Histogram of the faulty bands

We see that the value of Lsat is exceeded greatly in case of band 12, and in case of band 9, most of the values are around Lsat. As it was explained in the previous chapter (sec.5.1.2), these values correspond to the Lsat required for ocean applications. To correct this problem a modification was made to the process of data fusion, and not the upper boundary of Lsat was used. The results obtained with this change are shown in the next section.

5.2.3 Quality of the fused images with new upper boundary

It was tried to optimize the classification by changing the upper boundary to the highest value of radiance per MERIS band. Unfortunately, we did not dispose enough time to repeat the process of fusion for all the possible combinations. As a consequence, the process was repeated only for the combination previously selected: No regularization, no aggregation, 20 classes and window size 7 by 7 pixels. Thus, the new fused images were obtained and the same analysis made for the previous data was followed.

Now the ERGAS index, considering the 15 bands, has been improved, and also the statistic parameters, Bias, Correlation Coefficient, Standard Deviation and RMSE show

results very close to the ideal values that these parameters should have. Table 23 and figure 26 show these results.

Table 23: New values for ERGAS (Lsqlin_noagg,Class20,ws7)

Fused images no Lsat	ERGAS
18 February	2,953
16 April	3,366
6 June	2,190
14 July	3,263
6 August	2,236
9 August	2,647

*Graph 26.a Bias.

*Graph 26.b Correlation coefficient.

*Graph 26.c Standard Deviation. As previously, each color is representing a date, the original MERIS is marked with (*) and the fused image resampled to the MERIS pixel size with (.).

*Graph 26.d and e. RMSE absolute and normalized.

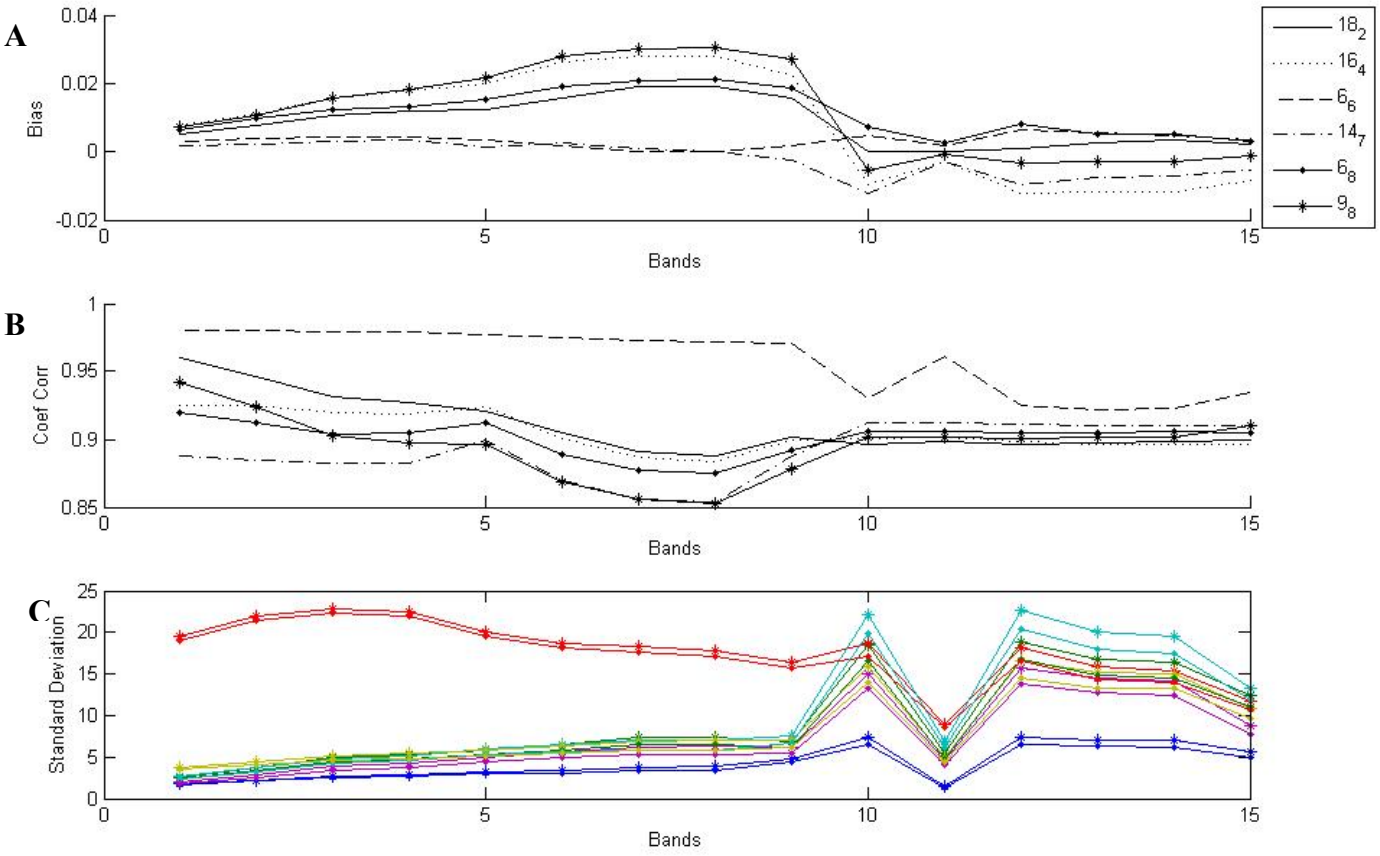

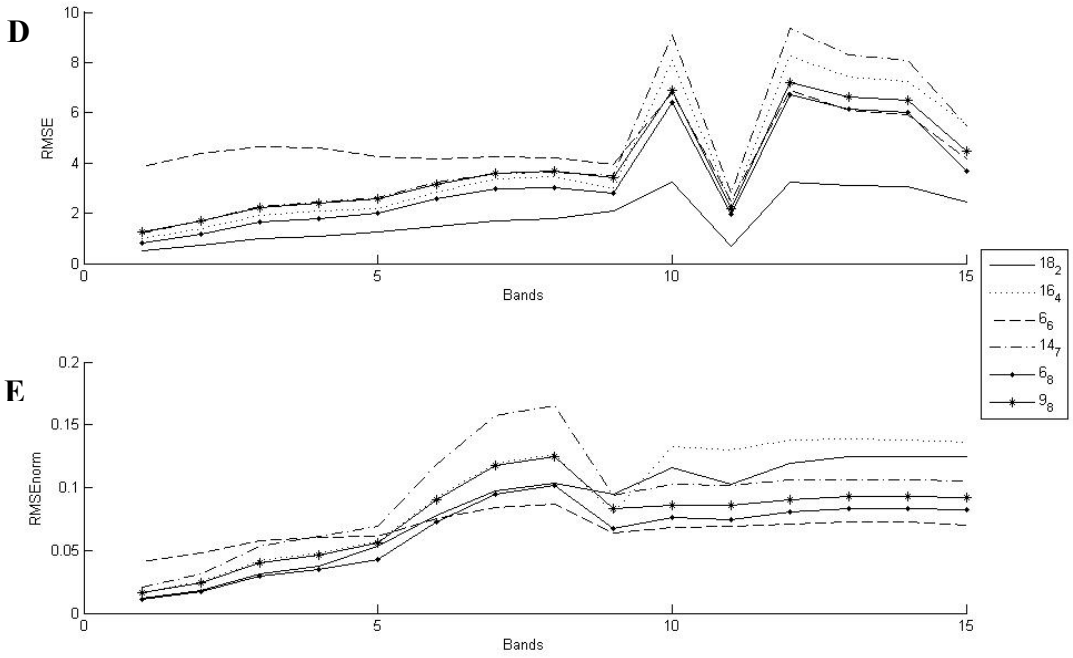

Figure 26: New values for a) Bias; b) Correlation coefficient; c) Standard deviation; d) RMSEabsolute; e) RMSEnormalized.

Subsequently, the classification of the fused images was made. The spectral signatures have been again obtained (figure 27). In this case bands 1, 2, 11 and 15 have been omitted, since for these bands all classes are affected by external effects. Bands 1 (412 nm) and 2 (442 nm) are affected by the atmosphere, band 11 (760 nm) by oxygen absorption and band 15 (900 nm) is influenced by water vapor absorption. Nevertheless, the overall accuracy of the new classified images has improved little with regard to the previous one. Neither the greenhouses have been included in this result, since when we have tried to classify them; the rest of the classes were confused with them.

Table 24: Overall accuracy and Kappa coefficients

Fused	***Overall accuracy***	***Kappa***	***Landsat***	***Overall accuracy***	***Kappa***
18 February	46.37%	0,3338	28 March	60.69%	0,5136
16 April	47.96%	0,3538			
06 June	45.83%	0,3608	10 July	61.76%	0,5208
14 July	48.33%	0,3257			
06 August	41.25%	0,2187	11 August	55.44%	0,4470
09 August	38.01%	0,1995			

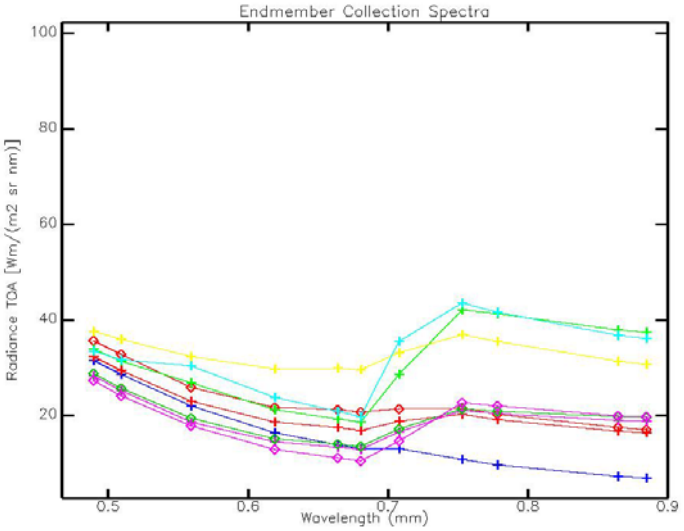

18th February

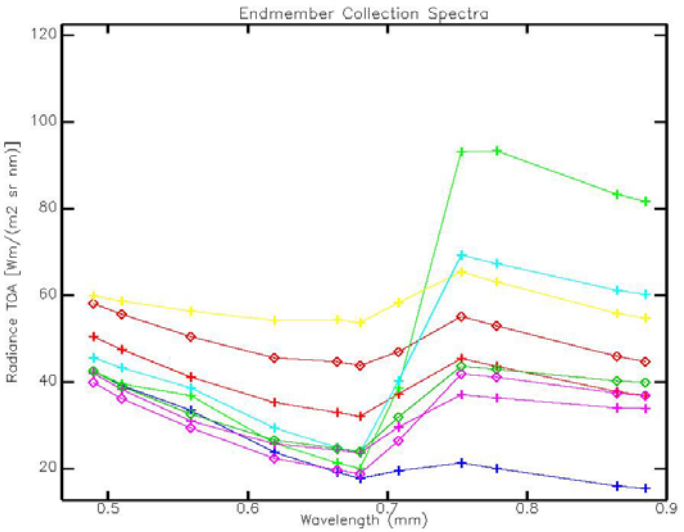

16th April

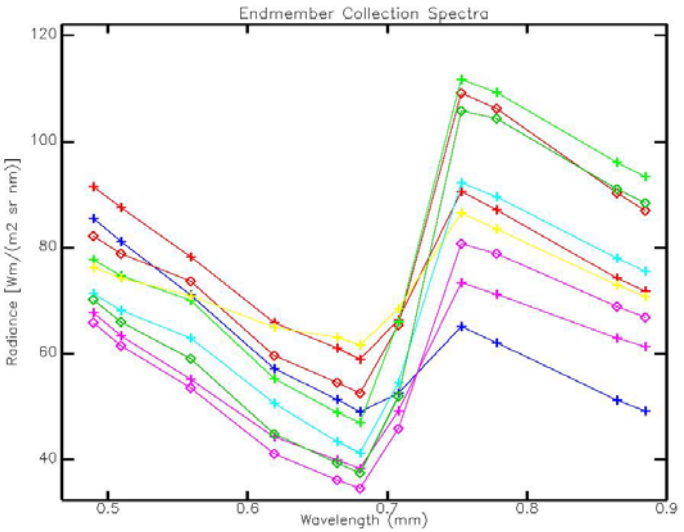

6th June

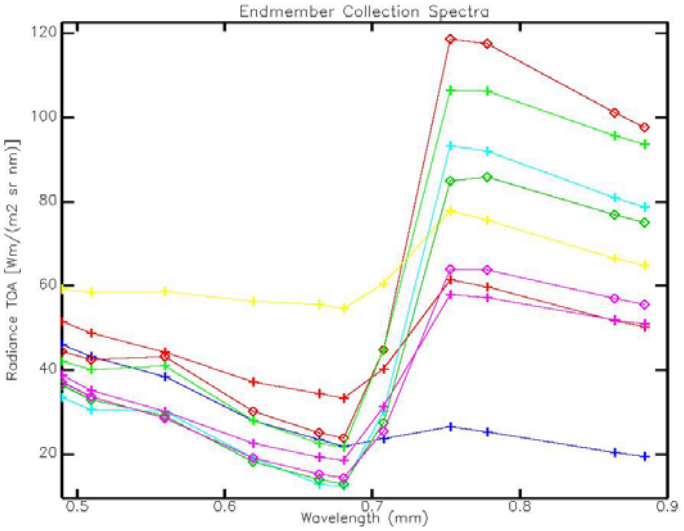

14th July

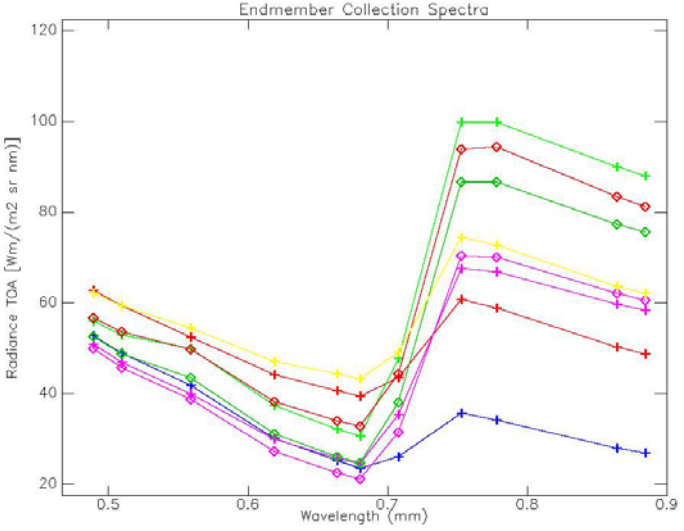

6th August

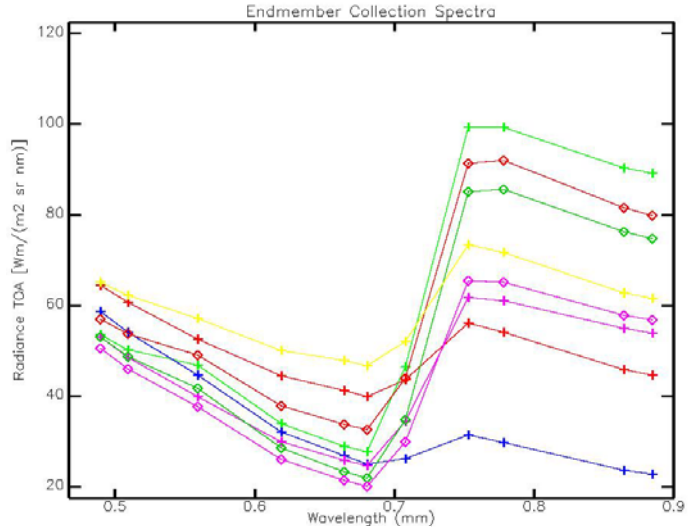

9th August

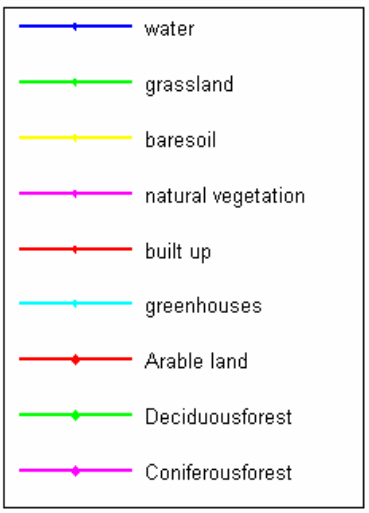

Figure 27: Spectral signature for the different dates.

We can check how the spectral signature for the greenhouses is quite mixed with the rest of the classes, being in truth a class with a spectral answer completely different to the rest of the class.
The first spectral profile, from 18th February, in this season of the year, the vegetation is not very vigorous, so it is normal that the spectral profile of many vegetation classes was quite similar to bare soil. In the case of images from 16th April and 14th July, the spectral profiles are more clear, classes as grassland, arable land or deciduous forest can be better distinguished. For this reason, the overall accuracy increases for these dates.
The poorest classification is coming from 6th June, 6th and 9th August. In the case, of the image from June, it has some clouds in the image coming from MERIS, and in the other two cases it is the Landsat image which presents some clouds from planes.

5.3 Conclusions and recommendations

The main purpose of this study was to check if there are advantages with regard to use a fused Landsat-TM and MERIS image over Landsat-TM image when mapping and monitoring land cover in The Netherlands. Nowadays, the LGN is based on Landsat TM images and a high amount of auxiliary data, which is an expensive task. If an accurate classification could be obtained with less extra-information, the process of land cover mapping would be easier and cheaper.
By checking the table 24, it is obvious that the best classification is given by Landsat TM images. However, some mistakes have been made during the research, and the initial parameters that were going to be optimized, have been chosen without the support of a solid criterion. How the data has been obtained and possible improvements will be commented next.

The first checking has been to observe how the conditional number of matrix "C" was affected when the application for the aggregation was included in the pre-processing to obtain the classified Landsat images for the fusion. Although it was supposed that the application would improve the quality of the fused image, it has not resulted in this way.

This fact can be explained, because the threshold has not been established under any criterion, and some points should have been taken into account. This threshold should depend on:

The number of classes in the classified image.
The maximum number of classes in a MERIS pixel.

A 10% of the MERIS pixel area is equivalent to 14.4 TM pixels (1 MERISpixel=144 TM pixels). When the TM image is classified in 80 classes, the maximum number of classes in a MERIS pixel is 57 for the Landsat image of 10th July (table 25). This means that there are around 3 pixels per class (144/57=2.53); thus with a threshold of 10 % many classes are being lost.

Table 25: Maximum number of classes per MERIS pixel

Tm7_280303		Tm5_100703		Tm5_110803	
Number class. in the image	Max class. in the pixel	Number class. in the image	Max class. in the pixel	Number class. in the image	Max class. in the pixel
10	10	10	10	10	10
20	19	20	20	20	20
30	28	30	28	30	28
40	32	40	35	40	33
60	41	60	48	60	48
80	49	80	57	80	52

Therefore the threshold should be lower.

The ERGAS values showed also, that a method without regularization gives better results than one applying regularization. A reason that could explain it is that the application "lsqlin" is a function that belongs to the "Optimization toolbox" of MATLAB®. This fact ensures us, that we are obtaining the best mathematical solution. However "NLCSmoothreg", the application proposed by Michael Wendlandt, maybe not a general application for all cases of ill-posed problems. Some reasons, why it could be failing, are:

- The input "guess": this parameter gives a first estimation for the values that the endmembers should have. A rough guess of the solution is being given with this parameter; however we do not know the solutions that can be obtained.
- It is not sure that the retrieval of parameter lambda was suitable.

Subsequently, to optimize the parameters in the method, the number of classes in the high spatial resolution image and the size of the window where the algorithm is applied was chosen by checking all the combinations with a MERIS and Landsat image. The chosen images were from 18th February (MERIS) and 28th March (Landsat TM). In this season of the year, classes like arable land, deciduous forest or grassland do not show a representative spectral profile of the vegetation, since they are mainly bare soil. It would have been more appropriate, to optimize these parameters with dates where the classes were better defined.

Also the problem with the values of Lsat has brought about that these parameters had not been optimized correctly. Only one combination was tested with a correct upper boundary, but it was not clear that it was the best combination to get the fused images.

Therefore it can not be stated that a fused image is not useful to map land cover since those variables were not correctly optimized. If the previous comments are taken into account for next researches, it could be possible to improve the obtained classifications.

6. Overall conclusions

This chapter summarizes the main conclusions of the two previous ones i.e. the justification of studying subpixel level and the process of data fusion.

Two methods have been tested to search the scale that gives the best visualization of the study area. To give a specific answer for this question is difficult since not all land covers present the same features and to find a appropriate common scale for all classes is not possible. But, the clear conclusion obtained is that the MERIS information has to be downscaled. An area of 300 by 300 m^2 is made up of many classes. The more restrictive scale was given by the class built up. Finally it was decided to downscale the MERIS information to the scale of Landsat TM, 25 m.
The indices CA, PLAND, NP and LSI have been used as indicative of the features of the landscape. CA and PLAND give information of abundance of each class in a specific landscape. The number of patches (NP) with regard to these indices and LSI show the distribution of each class, whether the class appears to be spread over the landscape or grouped in big patches.

Subsequently, a data fusion technique was applied between Landsat TM and MERIS image and some indices were computed to check the quality of these images. The main goal of this research was to check the accuracy that a classified fused image presents with regard to the classified image from a Landsat TM. The fused image has the spatial information of Landsat (25 m) and spectral information of MERIS (15 bands), so the fused image should contribute to improve the information that each individual image gives. However, the final results do not support this hypothesis. But, as it has been explained in the previous chapter, some problems were had during the analysis and the fused image has not been obtained with all the parameters correctly optimized.
One of the mistakes was the values of Lsat. When this values were changed the results obtained with regard to the previous one improved. The overall accuracy of the new classified images increases a 6 %. Therefore it is probably to get better fused images if the parameters are successfully optimized.
The quality of the fused images was checked with ERGAS and statistical parameters (i.e. correlation coefficient, standard deviation, bias). ERGAS is a good index, since it takes into account many measurements and presents good features that a quality index should have. However, it fails in measuring spectral distortion; for that reason the other statistical parameters were also computed. Visual analysis, although it can be subjective, is also useful in the quality assessment. When the fused images were visualized, dark pixels in one of the images made us to decide to choose a method without regularization.
To complement this research, some studys could be made in this area. For instance, studying multitemporal classification. Also to check if adding the middle infrared band (MIB) from Landsat to the fused image could improve the classification. Because, MERIS although has high spectral resolution, their bands are highly correlated.

After this discussion, we find that it is worthy to investigate the improvements that have been commented. If an accurate optimization is achieved, then the fused image can be a promising alternative for land cover mapping.

7. References

Acerbi-Junior, F. W., R. Z. Milla, J.G.P.W.Clevers, and M. E. Schaepman, 2005a, MODIS and Landsat TM image fusion using the SIFuLAP method for mapping the Brazilian savannas (Cerrado).

Acerbi-Junior, F. W., M. Wachowicz, and J. G.P.W.Clevers, 2005b, Are we using the right quality measures in multiresolution data fusion?

Aiazzi, B., S. Baronti, M. Selva, L. Alparone, A. Garzelli, and F. Nencini, 2004, Spectral information extraction by means of MS+PAN fusion: European Space Agency, (Special Publication) ESA SP, p. 143-150.

Amarsaikhan, D., and T. Douglas, 2004, Data fusion and multisource image classification: International Journal of Remote Sensing, v. 25, p. 3529-3539.

BEAM, 2005, Brockmann Consult.http://scipc3.scicon.gkss.de/services/beam2/software/.

Beauchemin, M., K. B. Fung, and X. Geng, A Method based on local variance for quality assessment of multiresolution image fusion http://www.isprs.org/commission3/proceedings/papers/paper055.pdf.

Billah, M., and G. A. Rahman, 2004, Land cover mapping of Khulna city applying remote sensing technique: Proc. 12th Int. Conf. on Geoinformatics-Geospatial Information Research:Briding the Pacific and Atlantic.

Borel, C. C., and S. A. W. Gerstl, 1994, Nonlinear Spectral Mixing Models for Vegetative and Soil Surfaces: Remote Sensing of Environment, v. 47, p. 403-416.

Bretschneider, T., and O. Kao, 2000, Image Fusion in Remote Sensing, Clausthal - Germany, Department of Computer Science - Technical University of Clausthal.

Carvalho, L. M. T. d., J. G. P. W. Clevers, A. K. Skidmore, and S. M. d. Jong, 2004, Selection of imagery data and classifiers for mapping Brazilian semideciduous Atlantic forests: International Journal of Applied Earth Observation and Geoinformation, v. 5, p. 173-186.

Chang, C. I., H. Ren, C. C. Chang, F. D'Amico, and J. O. Jensen, 2004, Estimation of subpixel target size for remotely sensed imagery: Ieee Transactions on Geoscience and Remote Sensing, v. 42, p. 1309-1320.

Chavez, P. S., S. C. Sides, and J. A. Anderson, 1991, Comparison of 3 Different Methods to Merge Multiresolution and Multispectral Data - Landsat Tm and Spot Panchromatic: Photogrammetric Engineering and Remote Sensing, v. 57, p. 295-303.

Clevers, J., H. Bartholomeus, M. Sander, and A. J. W. DE WIT, 2004a, Land Cover Classification with the medium resolution imaging spectometer (MERIS): EARSeL eProceedings, v. 3, p. 354-363.

Clevers, J. G. P. W., S. M. de Jong, G. F. Epema, F. van der Meer, W. H. Bakker, A. K. Skidmore, and E. A. Addink, 2002, MERIS and the red-edge position: International Journal of Applied Earth Observation and Geoinformation, v. 2001, p. 313-320.

Clevers, J. G. P. W., R. Z. Milla, M. E. Schaepman, and H. M. Bartholomeus, 2005, Using MERIS on ENVISAT for land cover mapping: European Space Agency, (Special Publication) ESA SP, p. 771-780.

Clevers, J. G. P. W., R. Zurita Milla, M. E. Schaepman, and H. M. Bartholomeus, 2004b, Use of MERIS data for land cover mapping in the Netherlands.

Congalton, R. G., and R. A. Mead, 1983, A Quantitative Method to Test for Consistency and Correctness in Photointerpretation: Photogrammetric Engineering and Remote Sensing, v. 49, p. 69-74.

Curran, P. J., and C. M. Steele, 2005, MERIS: The re-branding of an ocean sensor: International Journal of Remote Sensing, v. 26, p. 1781-1798.

De Wit, A. J. W., 2003, Land use mapping and monitoring in the Netherlands using remote sensing data: International Geoscience and Remote Sensing Symposium (IGARSS), p. 2614-2616.

De Wit, A. J. W., and J. G. P. W. Clevers, 2004, Efficiency and accuracy of per-field classification for operational crop mapping: International Journal of Remote Sensing, v. 25, p. 4091-4112.

ENVI, 2004, ENVI User´s Guide.

Fisher, P., 1997, The pixel: A snare and a delusion: International Journal of Remote Sensing, v. 18, p. 679-685.

Garguet-Duport, B., J. Girel, J.-M. Chassery, and G. Pautou, 1996, The use of multiresolution analysis and wavelets transform for merging SPOT panchromatic and multispectral image data: Photogrammetric Engineering and Remote Sensing, v. 62, p. 1057-1066.

González-Audícana, M., A. Seco, X. Otazu, and O. Fors, 2005, Comparison between Mallat's and the 'à trous' discrete wavelet transform based algorithms for the fusion of multispectral and panchromatic images: International Journal of Remote Sensing, v. 26, p. 595-614.

Grana, M., and A. D'Anjou, 2004, Feature extraction by linear spectral unmixing: Knowledge-Based Intelligent Information and Engineering Systems, Pt 1, Proceedings, v. 3213, p. 692-698.

Hansen, P. C., 2001, Regularization Tools Version 3.1 for Matlab 6.0: Numerical Algorithms, v. 6, p. 1-35.

Hill , J., 1999, A local correlation approach for the fusion of remote sensing data with different spatial resolutions in forestry applications.

Hyppänen, H., 1996, Spatial autocorrelation and optimal spatial resolution of optical remote sensing data in boreal forest enviroment: International Journal of Remote Sensing, v. 17, p. 3441-3452.

Klith Bøcher, P., 2003, Investigating the Potentials of the Spatial Domain in High-Resolution Imagery for Mapping Scale-Specific Structures of Forest Vegetation.: Ph.D. Thesis thesis, University of Aarhus, Denmark, 114 p.

Lillesand, T. M., and R. W. Keifer, 2000, Remote Sensing and Image Interpretation, New York: Wiley, 715 p.

Mather, P. M., 2004, Computer processing of remotely-sensed images: an introduction, New York: Wiley, 324 p.

Minghelli-Roman, A., M. Mangolini, M. Petit, and L. Polidori, 2001, Spatial resolution improvement of MeRIS images by fusion with TM images: Ieee Transactions on Geoscience and Remote Sensing, v. 39, p. 1533-1536.

Moran, M. S., 1990, A Window-Based Technique for Combining Landsat Thematic Mapper Thermal Data with Higher-Resolution Multispectral Data over Agricultural Lands: Photogrammetric Engineering and Remote Sensing, v. 56, p. 337-342.

Mucher, C. A., K. T. Steinnocher, F. P. Kressler, and C. Heunks, 2000, Land cover characterization and change detection for environmental monitoring of pan-Europe: International Journal of Remote Sensing, v. 21, p. 1159-1181.

Pajares, G., and J. M. de la Cruz, 2004, A wavelet-based image fusion tutorial: Pattern Recognition, v. 37, p. 1855-1872.

Park, J. H., and M. G. Kang, 2004, Spatially adaptive multi-resolution multispectral image fusion: International Journal of Remote Sensing, v. 25, p. 5491-5508.

Pellemans, A. H. J. M., R. W. L. Jordans, and R. Allewijn, 1993, Merging multispectral and panchromatic SPOT images with respect to the radiometric properties of the sensor: Photogrammetric Engineering & Remote Sensing, v. 59, p. 81-87.

Pohl, C., and J. L. Van Genderen, 1998, Multisensor image fusion in remote sensing: Concepts, methods and applications: International Journal of Remote Sensing, v. 19, p. 823-854.

Price, J. C., 1999, Combining multispectral data of differing spatial resolution: Ieee Transactions on Geoscience and Remote Sensing, v. 37, p. 1199-1203.

Ray, T. W., and B. C. Murray, 1996, Nonlinear spectral mixing in desert vegetation: Remote Sensing of Environment, v. 55, p. 59-64.

Robinson, G. D., H. N. Gross, and J. R. Schott, 2000, Evaluation of two applications of spectral mixing models to image fusion: Remote Sensing of Environment, v. 71, p. 272-281.

Rogan, J., and D. M. Chen, 2004, Remote sensing technology for mapping and monitoring land-cover and land-use change: Progress in Planning, v. 61, p. 301-325.

Simone, G., A. Farina, F. C. Morabito, S. B. Serpico, and L. Bruzzone, 2002, Image fusion techniques for remote sensing applications: Information Fusion, v. 3, p. 3-15.

Tapiador, F. J., and J. L. Casanova, 2002, An algorithm for the fusion of images based on Jaynes' maximum entropy method: International Journal of Remote Sensing, v. 23, p. 777-785.

Thomas, C., and L. Wald, 2005, Assessment of the quality of fused products: New Strategies for european Remote Sensing, Oluic, p. 10.

Thunnissen, H. A. M., and A. J. W. De Wit, 2000, The national land cover database of the Netherlands: Geoinformation for All; XIX Congress of the International Society for Photogrammetry and Remote Sensing (ISPRS), v. 33, p. 223-230.

Treitz, P., and J. Rogan, 2004, Remote sensing for mapping and monitoring land-cover and land-use change: Progress in Planning, v. 61, p. 267-+.

Van Der Meer, F. D., J. G. P. W. Devers, S. M. De Jong, W. H. Bakker, G. F. Epema, A. K. Skidmore, and K. Scholte, 2000, MERILAND: MERIS potential for land applications: USP-2 Report, v. 99.

Van Oort, P. A. J., A. K. Bregt, S. De Bruin, and A. J. W. De Wit, 2004, Spatial variability in classification accuracy of agricultural crops in the Dutch national land-cover database: INT. J. GEOGRAPHICAL INFORMATION SCIENCE, v. 18.

Verbyla, D. L., 1995, Satellite Remote Sensing of Natural Resources.

Verstraete, M. M., B. Pinty, and P. J. Curran, 1999, MERIS potential for land applications: International Journal of Remote Sensing, v. 20, p. 1747-1756.

Wald, L., 2002, Data Fusion Definitions and Architectures: Fusion of Images of Different Spatial Resolutions, Ecole des Mines Pres, 198 p.

Wendlandt, M., 2005, Non-Linear Constraint Smooth Regularization.

Woodcock, C. E., and A. H. Strahler, 1987, The Factor of Scale in Remote-Sensing: Remote Sensing of Environment, v. 21, p. 311-332.

www1, LGN web site: www.alterra.wur.nl/uk/cgi/LGN/.

www2, envisat.esa.int.

www4, www.amara.com/IEEEwave/IW_overview.html.

www5, http://www.library.cornell.edu/nr/bookcpdf/c2-6.pdf.

www6, http://mathworld.wolfram.com/.

www8, http://www.csc.noaa.gov/crs/rs_apps/sensors/landsat.htm.

www9, http://landsat.usgs.gov/programdesc.html.

Zhang, Y., 1999, A new merging method and its spectral and spatial effects: International Journal of Remote Sensing, v. 20, p. 2003-2014.

Zhang, Y., 2002, Problems in the fusion of commercial high-resolution satelitte images as well as Landsat 7 images and initial solutions: International Archives of Photogrammetry and Remote Sensing, v. 34.

Zhang, Y., 2004, Understanding image fusion: Photogrammetric Engineering and Remote Sensing, v. 70, p. 657-661.

Zhukov, B., D. Oertel, and F. Lanzl, 1995, Multiresolution multisensor technique for satellite remote sensing: International Geoscience and Remote Sensing Symposium (IGARSS), p. 51-53.

Zhukov, B., D. Oertel, F. Lanzl, and G. Reinhackel, 1999, Unmixing-based multisensor multiresolution image fusion: Ieee Transactions on Geoscience and Remote Sensing, v. 37, p. 1212-1226.

Zhukov, B., D. Oertel, and M. Lehner, 1997, TM/LANDSAT thermal image unmixing: Proceedings of SPIE - The International Society for Optical Engineering, p. 85-96.

Zurita Milla, R., M. E. Schaepman, J. G. P. W. Clevers, M. Kneubuchler, and S. Delwart, 2005, Long-term meris land product accuracy assessment based on vicarious calibration and regional validation: European Space Agency, (Special Publication) ESA SP, p. 63-71.

APPENDIX I: PROPOR_MAXCLASSES

```
function [propor,maxclasses]=Propor_maxclasses(XC,sw,ratio,I)

% The output of this function are propor and maxclasses.
% propor is a 3rD matrix of size MERIS image and such bands as number
% of classes
% maxclasses is a matrix of two columns where it is represented in the
% first column the different size of window (MERIS pixel) and in the
  second column the max number of classes in that window size.
% XC is number of classes
% sw is a vector with the different window sizes
% ratio is pixelSizeMERIS/pixelSizeLandsat_TM
% I is the classified Landsat image


% classes per pixel and proportions
[CL_pixel, propor,max_class_in_one_pixel]=ClassProportion(I,ratio,XC);

propor=single(propor);

clear I CL_pixel max_class_in_one_pixel

for ii=1:length(sw)
    % For processing with a sliding window of size sw*sw

ws=(sw(ii));

% computing the cond number, number of classes in a sw*sw MERIS window

[cond_number_matrix,number_classes_matrix]=Cond_numberclasses_nofractions(propor,ws);

% compute max number of classes in a sw*sw MERIS window
    maxclass=max(number_classes_matrix(:));
    maxclasses(ii,:)=[ws maxclass];

    clear number_classes_matrix cond_number_matrix
end

maxclasses
```

APPENDIX II: ClassProportion

```
Function
[CL_PIXEL,PROPORTIONS,MAXNUMCLASSES]=ClassProportion(I,WS,NumClasses)

    % This function has been created to get the proportion of the
    different
    % classes that there is when a MERIS pixel is overlaped on TM pixel
    %
    [CL_PIXEL,PROPORTIONS,MAXNUMCLASSES]=ClassProportion(I,WS,NumClasses)
    %
    % I is a classified TM image
    % WS is the window size (12*12)MERIS=300m ; TM=25m
    % WS is the sqrt of the number of TM pixels in a MERIS pixel
    % NumClasses is the number of classes in which TM has been classified
    % CL_PIXEL is a matrix where it is represented the amount of classes
    % into each MERIS pixel
    % PROPORTIONS is a multiband matrix where it is represented the
    % proportions of each class in each pixel. A band per class
    % MAXNUMCLASSES is the max number of classes there exist in a MERIS
    pixel


    % Size of TM image
    sizeI=size(I);

    % Size of the window
    n=WS;

    % Size of MERIS'image
    sizeML=[sizeI(1)/n sizeI(2)/n];

    %number of classes
    c=NumClasses;

    % blok processing
    CL_PIXEL= blkproc(I,[n n],@histc_ml,n,c,sizeML);

    disp('loading the propotion file')

    load ML2file;
    PROPORTIONS=ML2;

    delete ('ML2file.mat')

    MAXNUMCLASSES=max(CL_PIXEL(:));
```

APPENDIX III: Cond_number_nofractions

```
function
[cond_number_matrix,number_classes_matrix]=Cond_numberclasses_nofracti
ons(A,windowsize)


% A is the matrix where each class fractions is stored in a band
% The output will be FRACTIONS, matrices with pixels in lines and
% proportions in columns, the condition number of these matrices and
the % number of classes in each matrix.
% windowsize: sliding window
% nc is the number of classes of the classified image
% Conditional number similar to 1 means that the matrix is singular,
it % has linearly independent vector.
% number_classes in the pixels of the window


A;
sw=windowsize;
nc=size(A,3); % A is coming from ClassProportion.m and the number of
bands is the number of classes
a=(sw-1)/2;
AA=zeros((size(A,1)+(2*a)),(size(A,2)+(2*a)),nc);
AA((1+a):(size(AA,1)-a),(1+a):(size(AA,2)-a),:)=A;
B=zeros(sw,sw,nc); %initialising output1 (it is the cube that will be
transformed in a matrix)
contar=0; % init the counter

for i=1+a:size(AA,1)-a
    for j=1+a:size(AA,2)-a
        contar=contar+1;
        B=AA(i-a:1:i+a,j-a:1:j+a,:);

       % calling the function extract3rdD
        C=extract3rdD(B); % C has (sw*sw) rows and (nc) cols

        % To know the columns that are non-zero
        C=C(:,any(C));
       % To compute conditional number
        cond_number(contar)=cond(C);
        number_classes(contar)=size(C,2);

        % keep the C matrix (OUT OF MEMORY, because of that was
decided        % to remove it)
        % FRACTIONS=C;
    end
end

% changing to a matrix format
cond_number_matrix=reshape(cond_number,size(A,2),size(A,1))';
number_classes_matrix=reshape(number_classes,size(A,2),size(A,1))';

pack
```

APPENDIX IV: ZHUKOV_MMT

```
function
fused_image=Zhukov_MMT(sw,maxclasses,XC,propor,nbandMERIS,rootTM,rootM
ERIS,TM_classified,ratio,method)

%fused_image=Zhukov_MMT(sw,maxclasses,XC,propor,nbandMERIS,rootTM,root
ME% RIS,TM_classified,ratio,method)

% This function obtains a fused image aplying the methodology proposed
% by Zhukov et al. 1999
%
% The algoritm is executed in each pixel of the MERIS image by sliding
% window.
% sw is a vector with different window sizes.
% maxclasses is the maximum number of classes existing in the MERIS
% window
% XC is the number of classes in which the TM image has been
classified
% propor is a matrix coming of ClassProportion
% ratio=pixelsizeTM/pixelsizeMERIS
% method, four methods are proposed for solving the equation.Two of
them % apply regularization.
%
% Mariluz Guillén Climent
% 12-jul-2005
% V.01

% loop for each window size

for ii=1:length(sw)

% PS(possible solutios) is a matrix where is indicated the minimum
size % window that can solved a number of classes

  maxclass=maxclasses(ii,2);
    PS=possible_solutions(maxclass,sw(ii));
    if PS==1
        % padding of the proportions
        nc=size(propor,3); % the number of bands is the number of
classes
        a=(sw-1)/2; % frame that is going to be pad

% Cube of zeros
propor_pad=zeros((size(propor,1)+(2*a)),(size(propor,2)+(2*a)),nc);
% Matrix propr inside of the cube
propor_pad((1+a):(size(propor_pad,1)-a),(1+a):(size(propor_pad,2)-
a),:)=propor;

        % loop for each band of MERIS
        for bb=1:nbandMERIS
            %load the bb band of the MERIS image
            subsetband={'band',bb};
            %for each cut MERIS image
            dirMERIS='';

            [M]=multibandreadenvi2(fileMERIS,(subsetband));
            % getting the size of MERIS
            [nfilM ncolM]=size(M);

            % padding with NaN
```

```
            a=(sw-1)/2; % frame that is going to be pad
            Mpadded=zeros((nfilM+2*a),(ncolM+2*a)); % padding with
zeros
            Mpadded=Mpadded./Mpadded; % changing zeros to NaN
            warning off

           % putting the band inside the NaN matrix
            Mpadded((1+a):size(Mpadded,1)-a,(1+a):size(Mpadded,2)-
a)=M;

           % finding the MERIS elements
            mask=isfinite(Mpadded); %Real number is 1, NaN is 0.
            indicesmeris=find(mask==1);
            [filameris colmeris]=find(mask==1);

            % checking that the mask is correct
            if length(indicesmeris)== nfilM*ncolM %numel(M(:,:,bb))

                % init the output
                fused_window=zeros(ratio,ratio,nfilM*ncolM);

                % loop for all meris pixels

                for iii=1:length(indicesmeris)
                    clear endmembers indicesofclass
% Pixel Value
PV=pixvalue(Mpadded,sw,colmeris(iii),filameris(iii));
        %Files and columns are changed because the image has been
         transposed
% Fractions
[F,nameclasses]=fractions_pad(propor_pad,sw,filameris(iii),colmeris(iii))
;

        if method==1;% no regularization no upper-lower boundaries
                        endmembers=lsqnonneg(F,PV);
        elseif method==2;% no regularization yes upper-lower
boundaries
                        indicesPV=find(isnan(PV));
                        PV(indicesPV)=0;
                        lsat=max(max(M(:,:,bb);
                        lb=zeros(length(PV),1);
                        ub=ones(length(PV),1).*lsat;
                        endmembers=lsqlin(F,PV,[],[],[],[],lb,ub);

        elseif method==3;% yes regularization no upper-lower
boundaries
                        % regularisation Tikhonov
                        [U,s] = csvd(F);
                        reg_corner = l_curve(U,s,PV,'Tikh');
                        endmembers=maxent(F,PV,reg_corner);
        elseif method==4;% yes regularization yes upper-lower
boundaries
                        [U,s] = csvd(F);
                        reg_corner = l_curve(U,s,PV,'Tikh');
                        lb=zeros(size(F,2),1);
                        ub=ones(size(F,2),1)*lsat(bb);
                        guess=ones(size(F,2),1);
                        tols=1e-7;
                        tolg=1e-5;
                        maxiter=100;
                        indicesPV=find(isnan(PV));
```

```
                        PV(indicesPV)=0;

[endmembers,rho,eta]=NLCSmoothReg(PV,F,reg_corner,'TIK',guess,1e-7,1e-
5,100,'off',lb,ub);
                    end

                   % Getting the TM pixels belonging to the central
                   % MERIS pixel
             TM_window=window_blk_col(TM_classified, ratio, iii);
                    % convert to double
                    TM_window=double(TM_window);

                    % putting each endmember in its place
                    % number of classes MERIS for the central pixel of
                    % the kernel sw*sw

nameclasses_centralpixel=nameclasses(nameclasses>0);

                    for jj=1:length(nameclasses_centralpixel)

indicesofclass=find(TM_window==nameclasses_centralpixel(jj));
                        TM_window(indicesofclass)=endmembers(jj);
                    end


                    % storing all the fused windows of 12 by 12 by all
                    % meris pixels
                    % fused_window(:,:,iii)=TM_window_endmembers;

                    fused_window(:,:,iii)=TM_window;

                end

          % recompose the fused image
        fused_image(:,:)=recompose_fused_col(fused_window,[nfilM
ncolM]);
             else
                 disp('bad programmer!')
             end % closing the if

            workdir=pwd;
             % directory where the results are going to be stored
             newdir='';
             cd (newdir)

eval(['writeenvi(fused_image,''fused_',num2str(bb),'_',rootTM,'',num2s
tr(XC),'_',num2str(sw(ii)),'_',rootMERIS,'.bsq'')'])

              cd (workdir)
           % free some memory
              pack

         end % clossing bands

    else
        disp('not enough equations!')
    end % closing the if PS

end % clossing sw
```

APPENDIX V: Pixelvalue and fractions

```
function PV=pixvalue(Merispadded,windowsize,contadorfila,contadorcol)

% PV=pixvalue(Merispadded,windowsize,contadorfila,contadorcol)
%
% Merispadded is a band of the MERIS image already padded for the ws
%
% contador is from the image MERIS

% init the output in matrix format
temp=zeros(windowsize,windowsize);

 Merispadded=Merispadded';

a=(windowsize-1)/2;
temp=Merispadded([contadorfila-a:1:contadorfila+a],[contadorcol-
a:1:contadorcol+a]);
PV=temp(:);


function
[FRACTIONS nameclass]=fractions_pad(AA,windowsize,contadorfila,contadorcol)

% AA is the matrix where each class fractions is stored in a band
% (proportion matrix)
% windowsize: size of the (MERIS) sliding window
%
% FRACTIONS is a matrix where the proportions of each class per pixel
% are represented
% the number of pixels of a MERIS window are in lines and the number
of % classes in that window in columns
% nameclass is a vector where are represented the classes exist in
each % window

%initialising output1 (it is the cube that will be transformed in a
% matrix)
sw=windowsize;
nc=size(AA,3);
a=(sw-1)/2;

B=zeros(sw,sw,nc);
%cutting AA according to the windowsize
B=AA([contadorfila-a:1:contadorfila+a],[contadorcol-
a:1:contadorcol+a],:);
% calling the function extract3rdD
C=extract3rdD(B); % C has (sw*sw) rows and (nc) cols
% removing cols full of zeros=the classes that are not present in
% the C matrix
classespresent=any(C);% Vector with 0 if the class does not exist in
that MERIS window and 1 if the class exists
nameclass=[(1:nc).*classespresent];
FRACTIONS=C(:,any(C));
```

APPENDIX VI: QUALITY INDEXES function

```
%Ergasv3
% The index ERGAS is computed for each dates LandsatTM and MERIS with
a
% determinated number of classes and size window.

%Cleaning
ccc
% Inputs
pixelsizeMERIS=300;
nbandMERIS=15;
pixelsizeTM=25;
ratio=pixelsizeMERIS/pixelsizeTM;
%Number of classes
classLandsat=[20];
%size windows
MERISwindow=[7];
% method for resampling
method='mean';

%common root for the fused image
root_fused_bands='fused__';

% root of the different Classified Landsat images
rootTM{1}='tm7_280303_Class';
rootTM{2}='tm7_280303_Class';
rootTM{3}='tm5_100703_Class';
rootTM{4}='tm5_100703_Class';
rootTM{5}='tm5_110803_Class';
rootTM{6}='tm5_110803_Class';

% directory where fused images are stored
dirFused_band='F:\Fused_6images_20_7\';

% root of the different MERIS images
rootMERIS{1}='M_rad_MER_20030218';
rootMERIS{2}='M_rad_MER_20030416';
rootMERIS{3}='M_rad_MER_20030606';
rootMERIS{4}='M_rad_MER_20030714';
rootMERIS{5}='M_rad_MER_20030806';
rootMERIS{6}='M_rad_MER_20030809';

% The bands 9,12 and 14 are usually distorted the ERGAS index
%bands=[1 2 3 4 5 6 7 8 10 11 13 15];
% directory where MERIS images are stored
dirMERIS='C:\Documents and Settings\Mª Luz\Mis
documentos\MariLuz\WAGENINGEN\Imágenes\MERIS\MERIS_dec\';

%Initializing ERGAS. This column vector represents the index ERGAS for
each
%image in the diferent dates.
ERGAS_fusedImage=zeros(length(rootTM),1);

%Initializing the output. In each line is represented the RMSEnorm per
band
%of each LandsatTM and MERIS dates
RMSEmatrix=zeros(length(rootTM),nbandMERIS);
%RMSEmatrix=zeros(length(rootTM),length(bands)); %It is another option
if the bands 9,12 and 14 aren´t taken into account.
```

```
CC_matrix=zeros(length(rootTM),nbandMERIS);

countroots=0;
for root=1:length(rootMERIS) %loop for each image
    countroots=countroots+1;

    CTM=num2str(classLandsat);

    MW=num2str(MERISwindow);

    % making sure that in the first moment this number is equal to
zero
    temp1=0;

    counterbands=0;

    for bb=1:nbandMERIS % loop for all bands
   %for bb=1:length(bands) %loop for all bands unless 9,12 and 14
        counterbands=counterbands+1;

        % This is for load only a band of the fused image in each loop
        subsetband={'band',bb};
        %subsetband={'band',bands(bb)};

        % load the fused image band

fileFused_band=strcat(dirFused_band,root_fused_bands,rootTM{root},CTM,
'_',MW,'_',rootMERIS{root},'.bsq');

fused=multibandreadenvi2(fileFused_band,(subsetband));

        %removing the frame effect
        fused=remove_frame(fused,MERISwindow,ratio);
        fused=double(fused);

        % fused image to MERIS pixel size
        switch method
            case 'bicubic';

fused_resampled=imresize(fused,1/(pixelsizeMERIS/pixelsizeTM),'bicubic
');
            case 'mean'
                fused_resampled=blkproc(fused,[ratio ratio],@meanmv);
        end

        maxFR=max(fused_resampled(:));
        minFR=min(fused_resampled(:));
        meanFR=mean(fused_resampled(:));
        stdFR=std(fused_resampled(:));

        % load the MERIS image band
        fileMERIS=strcat(dirMERIS,rootMERIS{root},'.bsq');
        MERIS=multibandreadenvi2(fileMERIS,(subsetband));
        % removing frame for checking with fused_resampled image
        MERIS=remove_frame(MERIS,MERISwindow,1);
        MERIS=double(MERIS);
        max_MERIS=max(MERIS(:));
        min_MERIS=min(MERIS(:));
        mean_MERIS=mean(MERIS(:));
        std_MERIS=std(MERIS(:));
```

```
        cc=corr2(fused_resampled,MERIS);


        %root mean square error(rmse) between MERIS and
fused_resampled
        %image
        frmse=rmse_matrix(MERIS,fused_resampled);
        frmse2=frmse^2;
        mean_MERIS2=mean_MERIS^2;
        temp1=temp1+(frmse2/mean_MERIS2);

        % Checking if some band is distorting the ERGAS value
        RMSEnorm(counterbands)=frmse/mean_MERIS;
        RMSEabs(counterbands)=frmse;
        CorrCoef(counterbands)=cc;
        MEANBIAS(counterbands)=(mean_MERIS-meanFR);
        STD(counterbands,:)=[std_MERIS stdFR];

    end %closing bands

    %RMSE_matrix stores per line the RMSEnorm of the bands for the
    %different fused images
    RMSEmatrix(countroots,:)=RMSEnorm;
    RMSEmatrixABS(countroots,:)=RMSEabs;

    %Statistical parameters matrices store per line the statistic
    %results per band
    CC_matrix(countroots,:)=CorrCoef;
    MEANBIAS_matrix(countroots,:)=MEANBIAS;
    STD_matrix(:,countroots*2-1:countroots*2)=STD;

    % Calculating ERGAS

ERGAS=(100*(pixelsizeTM/pixelsizeMERIS))*sqrt((1/size(MERIS,3))*temp1)
;

    % ERGAS_fusedImage stores the ERGAS for each dates of TM
    % and MERIS image
    ERGAS_fusedImage(countroots,1)=ERGAS;


end %closing roots
```

APPENDIX VII: CONFUSION MATRICES

Landsat image from 28 March 2003

Class	Water %	Arableland%	Grassland%	Baresoil%	Natural vegetation%	Deciduous forest%	Coniferous forest%	Built-up%	Total %
Water %	72,81	0,01	0,17	1,27	0,02	0,08	0,05	0,15	3,21
Arable land %	1,31	38,44	4,48	10,59	1,05	0,64	0,27	5,42	11,31
Grassland %	2,84	18,5	67,11	4,08	0,76	9,74	1,04	10,29	30,4
Baresoil %	2,1	13,69	3,4	55,87	2,75	0,59	0,4	2,85	5,25
Natural Veg %	0,69	1,13	1,29	4,49	64,42	5,31	2,95	1,38	3,64
Deciduous Forest %	4,23	4,16	6,55	8,17	22,62	60,06	18,99	10,28	12,03
Coniferous Forest %	2,03	0,25	2,14	3,55	4,79	14,13	71,01	3,09	11,78
Built up %	14	23,81	14,86	12	3,59	9,45	5,27	66,56	22,38
Total %	100	100	100	100	100	100	100	100	100

Overall accuracy = (3022053/4979391) = 60,69 %; Kappa Coefficient= 0,5136

Landsat image from 10 July 2003

Class	Water %	Arableland%	Grassland%	Baresoil%	Natural vegetation%	Deciduous forest%	Coniferous forest%	Built-up%	Total %
Water %	67.91	0.01	0.08	0.40	0.05	0.03	0.05	0.04	2.95
Arable land %	11.15	45.27	16.91	7.40	1.01	6.75	1.62	11.81	19.16
Grassland %	2.57	26.80	62.10	4.46	3.46	9.77	1.20	7.05	30.14
Baresoil %	0.94	2.72	1.48	61.57	2.55	0.11	0.36	2.87	2.02
Natural Veg %	4.55	0.71	2.72	4.92	77.02	1.37	5.76	1.16	4.69
Deciduous Forest %	1.07	13.54	4.21	1.94	1.90	67.43	15.27	1.98	11.31
Coniferous Forest %	3.25	0.55	1.57	1.84	4.44	9.24	68.88	2.29	10.97
Built up %	8.57	10.40	10.92	17.46	9.58	5.31	6.86	72.79	18.76
Total %	100	100	100	100	100	100	100	100	100

Overall Accuracy = (3075391/4979391) = 61.76%; Kappa coefficient= 0.5208

Landsat image from 11 August 2003

Class	Water %	Arableland%	Grassland%	Baresoil%	Natural vegetation%	Deciduous forest%	Coniferous forest%	Built-up%	Total %
Water %	54.64	7.85	21.77	6.38	10.88	2.05	2.99	29.69	14.59
Arable land %	5.83	45.49	2.58	16.93	1.84	5.92	0.87	4.81	21.30
Grassland %	0.07	0.18	54.96	0.01	0.00	0.05	0.01	0.83	2.36
Baresoil %	26.84	35.92	8.46	64.21	19.01	16.89	4.64	25.51	32.70
Natural Veg %	2.50	2.14	1.33	0.71	58.28	1.59	7.81	2.55	4.35
Deciduous Forest %	2.65	4.25	3.17	9.29	1.26	54.44	13.57	2.10	9.52
Coniferous Forest %	7.33	4.05	7.42	2.42	8.52	19.06	70.04	5.85	14.94
Built up %	0.13	0.12	0.32	0.03	0.21	0.00	0.08	28.66	0.25
Total %	100	100	100	100	100	100	100	100	100

Overall Accuracy = (2354685/4247416) = 55.4381% ; Kappa=0.4770

Fused image from TM 28 March and MERIS 18 February

Class	Water %	Arableland%	Grassland%	Baresoil%	Natural vegetation%	Deciduous forest%	Coniferous forest%	Built-up%	Total %
Water %	62,14	0,8	1,74	2,57	0,08	0,35	0,22	1,2	3,69
Arable land %	0,71	26,75	2,28	1,1	0,65	1,18	0,37	3,11	7,51
Grassland %	7,13	28,38	52,83	7,78	3,28	14,25	3,72	17,2	29,51
Baresoil %	1,97	3,11	2,89	35,29	3,96	3,05	3,24	2,41	3,07
Natural Veg %	0,69	0,68	1,45	3,23	46,32	9,85	14,1	1,62	4,84
Deciduous Forest %	0,56	0,84	1,12	1,51	7,82	16,56	10,5	2,9	3,73
Coniferous Forest %	0,35	0,13	0,95	1,24	5,44	7,18	46,5	1,21	7,31
Built up %	26,45	39,31	36,74	47,27	32,46	47,58	21,3	70,3	40,34
Total %	100	100	100	100	100	100	100	100	100

Overall Accuracy = (2309773/4979391) = 46,39% ; Kappa Coefficient= 0,3338

Fused image from TM 28 March and MERIS 16 April

Class	Water %	Arableland%	Grassland%	Baresoil%	Natural Vegetation%	Deciduous forest%	Coniferous forest%	Built-up%	Total %
Water %	63,24	0,9	2,38	3,55	0,21	0,83	0,24	1,76	4,11
Arable land %	0,82	30,18	3,5	7,85	2,6	1,72	0,82	2,79	8,86
Grassland %	7,26	25,26	53,27	3,29	1,35	14,76	2,08	15,32	28,42
Baresoil %	1,07	1,28	1,11	32,82	2,48	1,48	1,39	1,42	1,44
Natural Veg %	0,26	0,54	1,44	3,11	51,93	13,73	14,46	1,81	5,28
Deciduous Forest %	0,83	2,83	1,86	2,36	9,93	16,27	11,68	2,97	4,67
Coniferous Forest %	0,42	0,08	0,92	2,02	5,07	6,75	47,14	1,09	7,33
Built up %	26,09	38,92	35,52	45	26,42	44,46	22,19	72,85	39,89
Total %	100	100	100	100	100	100	100	100	100

Overall Accuracy=(2388207/4979391)= 47,96%; Kappa Coefficient= 0,3538

Fused image from TM 10 July and MERIS 6 June

Class	Water %	Arableland%	Grassland%	Baresoil%	Natural Vegetation%	Deciduous forest%	Coniferous forest%	Built-up%	Total %
Water %	56,43	0,07	0,17	0,65	0	0,16	0,04	0,52	2,58
Arable land %	10,65	38,94	16,69	22,78	7,37	17,98	6,47	19,6	20,38
Grassland %	18,82	28,68	51,06	14,49	13,63	26,28	10,7	24,5	32,54
Baresoil %	0,01	0	0,06	28,66	0,42	0,01	0,63	0,03	0,26
Natural Veg %	0,05	0,07	0,87	3,06	56,6	1,7	7,47	0,72	3,25
Deciduous Forest %	0,34	1,53	2,04	0,82	2,32	20,21	12,4	1,53	4,31
Coniferous Forest %	0,24	0,08	0,86	1,27	7,79	5,43	44,1	1,03	6,88
Built up %	13,46	30,63	28,24	28,26	11,86	28,25	18,3	52,1	29,8
Total %	100	100	100	100	100	100	100	100	100

Overall Accuracy = (2282293/4979391)= 45,83% ; Kappa Coefficient=0.3068 .

Fused image from TM 10 July and 14 July

Class	Water %	Arableland%	Grassland%	Baresoil%	Natural Vegetation%	Deciduous forest%	Coniferous forest%	Built-up%	Total %
Water %	54.32	0.05	0.24	0.68	0.00	0.02	0.01	0.20	2.45
Arable land %	18.13	48.71	29.98	31.74	11.89	33.33	11.54	33.00	31.41
Grassland %	15.80	41.24	55.22	8.15	5.80	20.79	6.81	19.51	34.88
Baresoil %	0.00	0.00	0.13	33.45	1.63	0.06	0.67	0.02	0.35
Natural Veg %	0.14	0.26	1.00	1.71	52.24	3.70	8.38	0.87	3.48
Deciduous Forest %	0.27	0.39	0.57	0.97	2.42	11.99	8.66	0.89	2.42
Coniferous Forest %	0.59	0.34	1.11	1.89	9.33	11.95	49.06	1.24	8.20
Built up %	10.74	9.01	11.75	21.42	16.69	18.16	14.86	44.27	16.82
Total %	100	100	100	100	100	100	100	100	100

Overall Accuracy= (2406506/4979391) = 48.3293; Kappa Coefficient= 0.3257;

Fused image from TM 11 August and MERIS 6 August

Class	Water %	Arableland%	Grassland%	Baresoil%	Natural Vegetation%	Deciduous forest%	Coniferous forest%	Built-up%	Total %
Water %	24,02	5,91	8,62	4,33	15,76	4,56	3,94	11,2	8,5
Arable land %	45,21	52,26	29,79	47,05	26,57	37,9	26,2	42	43,68
Grassland %	3,24	2,25	46,8	1,53	0,88	1,11	1,03	4,51	3,82
Baresoil %	23,18	36,4	13,77	45,42	11,63	30,3	13,1	23,2	30,64
Natural Veg %	0,19	0,24	0,09	0,1	20,87	1,42	3,08	0,28	1,3
Deciduous Forest %	0,38	0,32	0,05	0,26	1,48	3,35	3,15	1,12	0,95
Coniferous Forest %	2,8	1,9	0,46	0,77	19,79	20,9	48,1	4,64	10,15
Built up %	0,99	0,73	0,41	0,54	3,01	0,55	1,46	13,1	0,94
Total %	100	100	100	100	100	100	100	100	100

Overall Accuracy= (1752207/4247416) = 41.2535 %; Kappa Coefficient= 0.2187;

Fused image from TM 11 August and MERIS 9 August

Class	Water %	Arableland%	Grassland%	Baresoil%	Natural Vegetation%	Deciduous forest%	Coniferous forest%	Built-up%	Total %
Water %	25,55	4,08	7,85	2,96	3,42	2,8	3,39	3,86	7,17
Arable land %	31,48	41,84	22,34	38,33	18,26	27,4	11,7	19,1	32,62
Grassland %	1,78	1,48	47,09	0,85	0,64	0,63	0,61	1,98	3,09
Baresoil %	32,86	48,25	19,34	55,39	24,57	50,4	31,6	39,8	43,07
Natural Veg %	0,19	0,27	0,07	0,06	23,94	0,86	2,95	0,59	1,34
Deciduous Forest %	0,06	0,1	0,01	0,06	0,12	1,83	0,85	0,04	0,3
Coniferous Forest %	1,23	0,91	0,24	0,26	9,78	12,4	35,2	2,16	6,74
Built up %	6,83	3,07	3,07	2,08	19,27	3,71	13,7	32,5	5,66
Total %	100	100	100	100	100	100	100	100	100

Overall Accuracy=(1614593/4247416)= 38,01% ; Kappa Coefficient = 0,1995

APPENDIX VIII: Mathematical concepts

Singular value

A matrix "A" can be decomposed into so-called eigenvalues and eigenvectors, being a special set of scalars and vectors associated with a linear system of equations respectively.

$$A = P \cdot D \cdot P^{-1}$$

Equation 9: Matrix diagonalization

Where:
P is a matrix composed of the eigenvectors of A and P^{-1} the inverse of P.
D is the diagonal matrix constructed by the eigenvalues.

The square roots of the eigenvalues are the singular values.

Singular value decomposition

Any $m \times n$ matrix A whose number of rows m is greater than or equal to its number of columns n, can be written as the product of an $m \times n$ orthogonal matrix U, an $n \times n$ diagonal matrix S whose elements are the singular values of the original matrix and the transpose of an $n \times n$ orthogonal matrix V.

$$A = U \cdot s \cdot V'$$

Equation 10: Singular value decomposition

Singular value decomposition is used in some occasion like a method for solving most linear least-squares problems (www5).

Conditional number

The condition number of a matrix measures the sensitivity of the solution of a system of linear equations to errors in the data; it estimates the loss of precision in solving a linear system with that matrix. It is the ratio "*C*" of the largest to smallest singular value in the singular value decomposition of a matrix.
A system is said to be singular if the condition number is infinite, and ill-conditioned if it is too large. Values of condition number near 1 indicate a well-conditioned matrix (www6).
The large condition number implies that the columns of A are nearly linearly dependent (Hansen, 2001). One or more small singular values implies that A is nearly rank deficient, and the vectors V_i associated with the small singular values are numerical null-vectors of A.

Regularization

The term of regularization appears when we have problems with an ill-posed matrix. The ill-conditioning of the matrix does not mean that a meaningful approximate cannot be computed. Rather, it implies that standard methods in numerical linear algebra cannot be used in a straightforward manner to compute such a solution. Instead other

methods must to be applied in order to ensure the computation of a meaningful solution, and this is the goal of regularization methods.
In our case, for solving the equation 1, four methods have been proposed and two of them apply regularization methods. The most common method of regularization is the one known as Thikonov regularization, where the regularized solution x_λ is defined as the minimum of the following weighted combination of residual norm and the side constraint where the regularization parameter λ controls the weight given minimization of the side constraint relative to minimization of the residual norm.

$$x_\lambda = \arg\min\left\{\|Ax-b\|_2^2 + \lambda^2\|L(x-x^*)\|_2^2\right\}$$

Thus, the regularization parameter λ is a parameter which controls the properties of the regularized solution. For obtaining this parameter, a method called L-curve can be used (Hansen, 2001).

The L-curve is a graphical tool for analysis of discrete ill-posed problems. It is a plot for all valid regularization parameter, of the (semi)norm $\|Lx_{reg}\|_2$ of the regularized solution versus the corresponding residual norm $\|Ax_{reg}-b\|_2$. In this way the L curve displays the compromise between minimization of these two quantities, which is the main aim of the regularization methods.

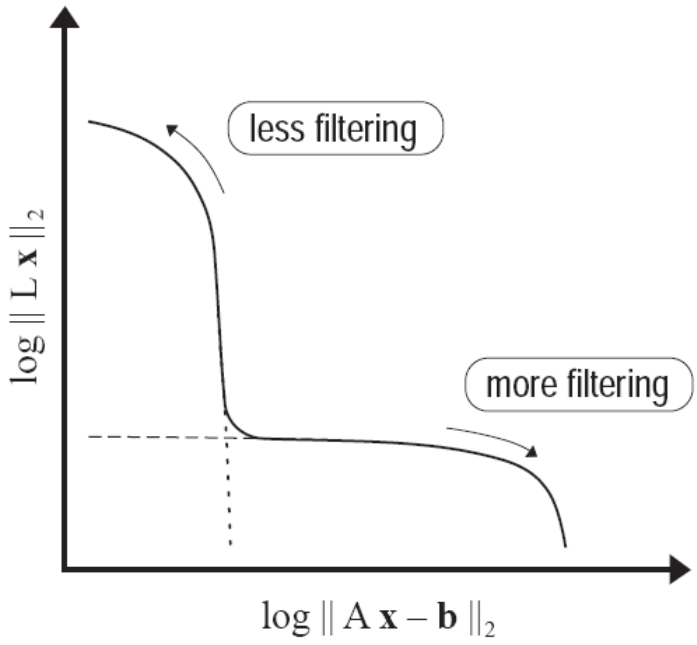

Figure 28: The generic form of the L-curve